# SciRE-Solver: Efficient Sampling of Diffusion Probabilistic Models by Score-integrand Solver with Recursive Derivative Estimation

## Shigui Li<sup>1\*</sup>

School of Mathematics
South China University of Technology
Guangzhou 510641, China
lishigui@mail.scut.edu.cn

#### Wei Chen<sup>1</sup>

School of Mathematics
South China University of Technology
Guangzhou 510641, China
maweichen@mail.scut.edu.cn

## Delu Zeng<sup>2†</sup>

School of Electronic and Information Engineering South China University of Technology Guangzhou 510641, China dlzeng@scut.edu.cn

#### **Abstract**

Diffusion probabilistic models (DPMs) are a powerful class of generative models known for their ability to generate high-fidelity image samples. A major challenge in the implementation of DPMs is the slow sampling process. In this work, we bring a high-efficiency sampler for DPMs. Specifically, we propose a score-based exact solution paradigm for the diffusion ODEs corresponding to the sampling process of DPMs, which introduces a new perspective on developing numerical algorithms for solving diffusion ODEs. To achieve an efficient sampler, we propose a recursive derivative estimation (RDE) method to reduce the estimation error. With our proposed solution paradigm and RDE method, we propose the score-integrand solver with the convergence order guarantee as efficient solver (SciRE-Solver) for solving diffusion ODEs. The SciRE-Solver attains state-of-the-art (SOTA) sampling performance with a limited number of score function evaluations (NFE) on both discrete-time and continuous-time DPMs in comparison to existing trainingfree sampling algorithms. Such as, we achieve 3.48 FID with 12 NFE and 2.42 FID with 20 NFE for continuous-time DPMs on CIFAR10, respectively. Different from other samplers, SciRE-Solver has the promising potential to surpass the FIDs achieved in the original papers of some pre-trained models with a small NFEs. For example, we reach SOTA value of 2.40 FID with 100 NFE for continuous-time DPM and of 3.15 FID with 84 NFE for discrete-time DPM on CIFAR-10, as well as of 2.17 (2.02) FID with 18 (50) NFE for discrete-time DPM on CelebA 64×64.

#### 1 Introduction

Diffusion probabilistic models (DPMs) [1–3] are a powerful class of generative models and have recently gained significant attention for their competitive performance on various tasks, including image generation [4, 5], text-to-image generation[6], video synthesis[7], and voice synthesis[8, 9]. DPMs are composed of two diffusion stages, the forward and reverse stages. In the forward stage,

<sup>\*</sup>Code is available at https://github.com/ShiguiLi/scire-solver

<sup>†</sup>Corresponding author

the input data is gradually perturbed over several steps by the addition of Gaussian noise, without any training. The primary purpose of this stage is to introduce randomness to gradually perturb the data distribution. The reverse stage of DPMs is tasked at recovering the original input data from the diffused (noisy) data by learning to gradually reverse the forward diffusion process, step by step. The reverse diffusion is a critical component of DPMs, as it allows the model to perform denoising on corrupted input data or generate samples from the learned data distribution.

In contrast to generative adversarial networks (GANs) [10] and variational auto-encoders (VAEs)[11], which necessitate the training of both forward and backward processes, DPMs learn models by emulating the ground-truth inverse process of a fixed forward process without the requirement to learn an encoder process. Additionally, DPMs are able to calculate the exact likelihood [3] by connecting neural ODEs [12], while also can achieve better sample quality for image generation [4] compared to GANs and VAEs. However, to generate high-fidelity samples, DPMs typically require several hundreds or even thousands of sequential steps of large-scale neural network evaluations to perform iterative generation or denoising [2], which leading to a slower sampling rate than single-step GANs or VAEs [13]. Therefore, it is crucial to develop efficient sampling methods for DPMs to enable their more efficient deployment in downstream applications. There are two main categories of existing

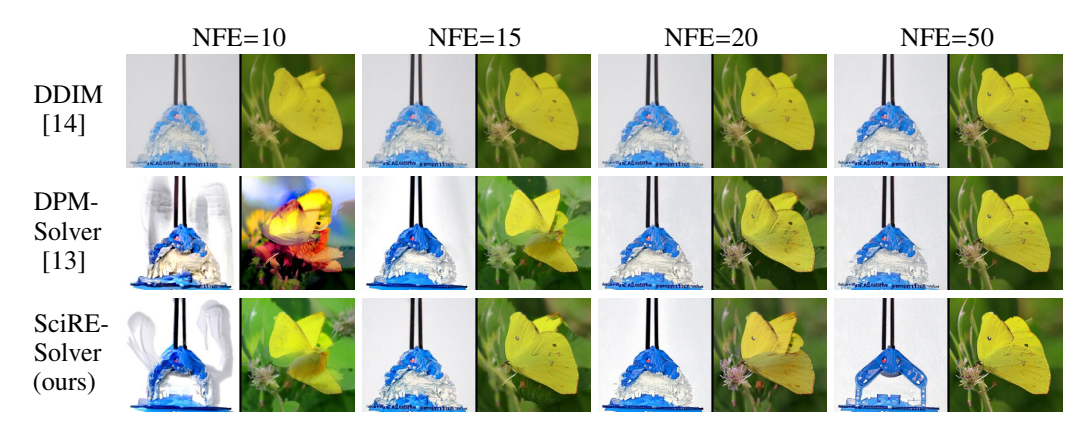


Figure 1: Random samples with the same random seed were generated by DDIM [14] (uniform time steps), DPM-Solver [13] (logSNR time steps), and SciRE-Solver (NSR time steps) with the same codebase, employing the pre-trained DPM [4] on ImageNet 256×256 (classifier scale: 2.5).

fast samplers for DPMs: training-based methods and training-free methods. While training-based methods, such as knowledge distillation[15–17] and consistency models [18], noise level learning[19], training sampler[20], or combining with other generative models[21–23] to obtain a fast sampler, they require an extra training stage, which can make it challenging to efficiently sample from an arbitrary pre-trained DPMs. On the other hand, training-free methods aim to accelerate the sampling process without an extra training stage, offering greater flexibility for use with various models and applications, including both unconditional and conditional sampling. The present training-free fast sampling methods are primarily devised based on diffusion ODEs, which are derived from the fact that the sampling process of DPMs can be reformulated as solving the corresponding diffusion ODE, as demonstrated by DDIM [14] and Score-SDE [3]. There are some fast sampling algorithms with training-free. PNDM [24] transformed the iterative formulation of DDIM into a derivative form, which was then solved using linear multistep (explicit Adams) methods. Furthermore, ERA-Solver [25] explored the use of implicit Adams methods for fast sampling. DPM-Solver [13] introduced exponential integrator for discretizing Diffusion ODEs from ODE literature [26], which leverages the semilinear structure of the learned diffusion process to reduce the discretization error. Additionally, DPM-Solver required extra network evaluations to observe intermediate noise terms for approximating Taylor expansion [27] in the sampling process. In contrast to the DPM-Solver, DEIS [28] proposed a fast sampler for DPMs by introducing an exponential integrator and combining RK-methods and Adams-Bashforth methods.

In this work, we have advanced the sampling efficiency of the training-free sampling method to a new level. In summary, the main contributions of this paper are as follows:

• We propose **score-based exact solution** paradigm to the diffusion ODEs as in Proposition 3.1, which bring a new perspective of developing numerical algorithms for solving diffusion ODEs.

- To reduce estimation errors, we introduce a **recursive derivative estimation** method that estimates the derivatives of the score function evaluation at the required evaluation points by recursively leveraging information from higher-order derivative terms to lower-order ones, as illustrated in Fig. 2.
- We propose **SciRE-Solver-k** (k = 2,3) with the convergence order guarantee, an efficient specialized solver with training-free, to tackle the problem of efficient sampling from DPMs.

Numerical experiments report that SciRE-Solver can efficiently generate high-quality samples on different datasets. Such as, we achieve 2.42 FID with 20 NFE for the continuous-time model and 3.67 FID with 20 NFE for the discrete-time model on CIFAR-10 dataset, 2.17 FID with 18 NFE for the discrete-time model on CelebA 64×64 dataset. SciRE-Solver has also shown promising potential to surpass the FIDs achieved in the original papers of some pre-trained models. For example, we achieve 3.15 FID with 84 NFE for discrete-time model and 2.40 FID with 100 NFE for continuous-time model on CIFAR-10 dataset, as well as 2.02 FID with 50 NFE on CelebA 64×64.

#### 2 Diffusion Probabilistic Models

The central goal of generative modeling is to establish a reliable and precise representation of the true data distribution  $p(\mathbf{x})$  based on a given set of observed samples  $\mathbf{x}$ . The diffusion probabilistic model uses a predetermined stochastic forward process (or noise schedule) to gradually add noise into the data, transforming the data distribution into a simple distribution (such as standard Gaussian distribution). Simultaneously, the models are trained to simulate the ground-truth inverse process of this forward process, gradually removing the noise from the data to recover the observed samples. A Markov sequence  $\{\mathbf{x}_t\}_{t\in[0,T]}$  with T>0 starting with  $\mathbf{x}_0$ , in the forward diffusion process of DPMs for D-dimensional data, is defined by the transition distribution

$$q(\mathbf{x}_t \mid \mathbf{x}_{t-1}) := \mathcal{N}(\mathbf{x}_t; \beta_t \mathbf{x}_{t-1}, (1 - \beta_t^2) \mathbf{I}), \tag{2.1}$$

where  $\beta_t \in \mathbb{R}^+$  is the variance schedule function [2], which is differentiable w.r.t t and possesses a bounded derivative. Given the transition distribution in Eq. (2.1), one can formulate the transition kernel of noisy data  $\mathbf{x}_t$  conditioned on clean data  $\mathbf{x}_0$  as

$$q(\mathbf{x}_t \mid \mathbf{x}_0) = \mathcal{N}(\mathbf{x}_t; \alpha_t \mathbf{x}_0, \sigma_t^2 \mathbf{I}), \tag{2.2}$$

where  $\alpha_t = \prod_{i=1}^t \beta_i$ ,  $\sigma_t = \sqrt{1 - \alpha_t^2}$  for the variance-preserving setting. DPMs choose *noise schedules* for  $\alpha_t$  and  $\sigma_t$  to ensure that the *marginal distribution*  $q_T(\mathbf{x}_T)$  approximates  $\mathcal{N}(\mathbf{x}_T; \mathbf{0}, \hat{\sigma}^2 \mathbf{I})$  for  $\hat{\sigma} > 0$ . In [29], Kingma et al. established the equivalence between the transition kernel of the following stochastic differential equation (SDE) and the one in Eq. (2.2) for  $\forall t \in [0, T]$ :

$$d\mathbf{x}_t = f(t)\mathbf{x}_t dt + g(t)d\omega_t, \quad \mathbf{x}_0 \sim q_0(\mathbf{x}_0), \tag{2.3}$$

where  $\omega_t \in \mathbb{R}^D$  denotes a standard Wiener process, and

$$f(t) = \frac{\mathrm{d}\log\alpha_t}{\mathrm{d}t}, \quad g^2(t) = \frac{\mathrm{d}\sigma_t^2}{\mathrm{d}t} - 2\frac{\mathrm{d}\log\alpha_t}{\mathrm{d}t}\sigma_t^2. \tag{2.4}$$

Further, Song et al. [3] demonstrated with some regularity conditions that the forward process in Eq. (2.2) has the following equivalent reverse process (*reverse SDE*) from time *T* to 0:

$$d\mathbf{x}_{t} = \left[ f(t)\mathbf{x}_{t} - g^{2}(t)\nabla_{\mathbf{x}}\log q_{t}\left(\mathbf{x}_{t}\right) \right] dt + g(t)d\overline{\omega}_{t}, \quad \mathbf{x}_{T} \sim q_{T}\left(\mathbf{x}_{T}\right), \tag{2.5}$$

where  $\overline{\omega}_t$  represents a standard Wiener process in the reverse time. Based on the reverse SDE in Eq. (2.5), Song et al. [3] derived the following ODE:

$$\frac{\mathrm{d}\mathbf{x}_{t}}{\mathrm{d}t} = f(t)\mathbf{x}_{t} - \frac{1}{2}g^{2}(t)\nabla_{\mathbf{x}}\log q_{t}(\mathbf{x}_{t}), \quad \mathbf{x}_{T} \sim q_{T}(\mathbf{x}_{T}),$$
(2.6)

where  $\mathbf{x}_t$  has a marginal distribution  $q_t(\mathbf{x}_t)$ , which is equivalent to the marginal distribution of  $\mathbf{x}_t$  of the SDE in Eq. (2.5). By substituting the trained noise prediction model  $\epsilon_{\theta}(\mathbf{x}_t, t)$  for the scaled score function:  $-\sigma_t \nabla_{\mathbf{x}} \log q_t(\mathbf{x}_t)$ , Song et al. [3] defined the following diffusion ODE for DPMs:

$$\frac{\mathrm{d}\mathbf{x}_{t}}{\mathrm{d}t} = f(t)\mathbf{x}_{t} + \frac{g^{2}(t)}{2\sigma_{t}}\boldsymbol{\epsilon}_{\theta}\left(\mathbf{x}_{t}, t\right), \quad \mathbf{x}_{T} \sim \mathcal{N}\left(\mathbf{0}, \hat{\sigma}^{2} \boldsymbol{I}\right). \tag{2.7}$$

Therefore, one can also generate samples by solving the diffusion ODE from *T* to 0 numerically. Compared to SDEs, ODEs can be addressed using larger step sizes since they are deterministic and do not involve stochasticity. Therefore, efficient numerical ODE solvers can be used to accelerate sampling. For example, Song et al. [3] employed the RK45 ODE solver [30] to solve the diffusion ODE. By ~ 60 NFE on the CIFAR-10 dataset, they achieved a quality comparable to solving Eq. (2.5) using 1000 NFE. Lu et al. [13] obtained a solution paradigm for diffusion ODEs using the *variation of constants* formula, and then discussed its exponential integral form of Taylor expansion. On the CIFAR-10 dataset, their proposed DPM-Solver achieved a generated quality of 2.87 FID, with only 20 NFE using the continuous noise prediction model. However, the solution form provided by the DPM-Solver may limit the flexibility in developing new numerical methods, as it often requires the use of exponential integrators in numerical algorithm design. Additionally, while the DPM-Solver can achieve good generation quality by using a small NFEs, the best results of the DPM-Solver still exhibit certain discrepancies compared to the results of the 1000-step SDE solver. Therefore, the development of efficient solvers is a highly meaningful and challenging task in order to further improve the sampling efficiency and enhance the generative capability of DPMs.

## 3 Score-integrand Solver with Recursive Derivative Estimation

In this section, we propose score-based exact solution paradigm for solving diffusion ODEs. In order to obtain an efficient sampling algorithm, we propose a recursive derivative estimation method to reduce the estimation error. Based on these results, we propose the score-integrand solver with guaranteed convergence order for solving diffusion ODEs.

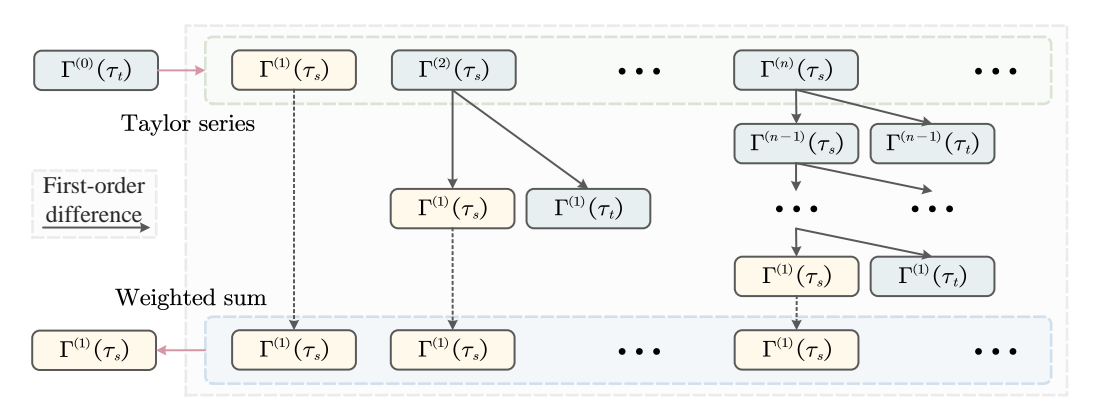


Figure 2: Schematic diagram of the *recursive derivative estimation method* tailored for score-integrand. Here we denote  $\epsilon_{\theta}^{(k)}\left(\mathbf{x}_{\psi(\tau)},\psi(\tau)\right)$  as  $\Gamma^{(k)}(\tau)$  for simplicity, as explained in Appendix C. The diagram exhibits an example of the derivative process of  $\Gamma^{(1)}(\tau_s)$  with  $\Gamma^{(0)}(\tau_t)$  given as input. Similarly, we can obtain the  $\Gamma^{(k)}(\tau_s)$ ,  $\forall k \in \mathbb{Z}_+$  with  $\Gamma^{(0)}(\tau_t)$  as input using analogous procedures.

#### 3.1 Exact solutions of Diffusion ODEs based on Score integration

Inspired by the *variation-of-constants* formula used in the DPM-Solver[13], the exact solution of the semi-linear ODE as Eq. (2.7) can be formulated by the *variation-of-constants* formula [31]:

$$\mathbf{x}_{t} = e^{\int_{s}^{t} f(\gamma) d\gamma} \left( \int_{s}^{t} h(\gamma) \boldsymbol{\epsilon}_{\theta} \left( \mathbf{x}_{\gamma}, \gamma \right) d\gamma + \mathbf{x}_{s} \right), \tag{3.1}$$

where  $h(\gamma) := e^{-\int_s^{\gamma} f(z) dz} \frac{g^2(\gamma)}{2\sigma_{\gamma}}$ , and  $\mathbf{x}_s$  represents the given initial value. Since  $f(\gamma) = \frac{d \log(\alpha_{\gamma})}{d\gamma}$ , thus  $h(\gamma) = \frac{\alpha_s}{\alpha_{\gamma}} \frac{g^2(\gamma)}{2\sigma_{\gamma}}$ . We observe that  $h(\gamma)$  can be rewritten as

$$h(\gamma) = \frac{\alpha_s}{2\alpha_{\gamma}\sigma_{\gamma}} \left( \frac{d\sigma_{\gamma}^2}{d\gamma} - 2 \frac{d\log\alpha_{\gamma}}{d\gamma} \sigma_{\gamma}^2 \right) = \frac{\alpha_s}{\alpha_{\gamma}} \left( \frac{d\sigma_{\gamma}}{d\gamma} - \frac{\sigma_{\gamma}}{\alpha_{\gamma}} \frac{d\alpha_{\gamma}}{d\gamma} \right) = \alpha_s \frac{dNSR(\gamma)}{d\gamma}, \tag{3.2}$$

where  $NSR(\gamma) := \frac{\sigma_{\gamma}}{\alpha_{\gamma}}$ , and we refer to it as the time-dependent *noise-to-signal-ratio* (*NSR*) function. Note that  $\frac{1}{NSR^2}$  is the signal-to-noise-ratio function defined in [29]. Then, we can rewrite Eq. (3.1) as

$$\mathbf{x}_{t} = \frac{\alpha_{t}}{\alpha_{s}} \mathbf{x}_{s} + \alpha_{t} \int_{s}^{t} \frac{d\mathrm{NSR}(\gamma)}{d\gamma} \boldsymbol{\epsilon}_{\theta} \left( \mathbf{x}_{\gamma}, \gamma \right) d\gamma. \tag{3.3}$$

Eq. (3.3) implies that the solution of the diffusion ODE can be decomposed into a linear part and a nonlinear part. The linear part can be computed analytically, while the remaining nonlinear part is an integral involving the neural network of score function evaluations. Compared with directly numerically solving the diffusion ODE, such decomposition method can reduce numerical errors and improve calculation accuracy because the linear part can be analytically computed.

The inverse function  $rNSR(\cdot)$  can be defined by letting  $\gamma = rNSR(NSR(\gamma))$ , based on the monotonically of NSR function w.r.t. time. Then, we obtain the most simplified exact solution formula for the diffusion ODEs so far by using the *change-of-variable* for NSR( $\gamma$ ) to Eq. (3.3).

**Proposition 3.1** Let  $\mathbf{x}_s$  be a given initial value at time s > 0. Then, the solution  $\mathbf{x}_t$  at time t of the desiffusion ODEs in Eq. (2.7) satisfies

$$\frac{\mathbf{x}_t}{\alpha_t} - \frac{\mathbf{x}_s}{\alpha_s} = \int_{\text{NSR}(s)}^{\text{NSR}(t)} \boldsymbol{\epsilon}_{\theta} \left( \mathbf{x}_{\text{rNSR}(\tau)}, \text{rNSR}(\tau) \right) d\tau. \tag{3.4}$$

See Appendix B for detailed derivation. As the integral term in the r.h.s. of Eq. (3.4) is solely dependent on the evaluation network  $\epsilon_{\theta}(\mathbf{x}_s, s)$  of scaled score function, we refer to such simplified exact solution form as *score-based exact solution* of diffusion ODEs. Note that score-based exact solution form is merely an integral expression in theory for which we do not actually know its specific exact solution. Fortunately, we observe that the score-based exact solution form presents a fresh insight towards developing numerical methods for solving diffusion ODEs, as this exact solution form formulates a numerical solving format different from the DPM-Solver [13], as detailed in Section 3.4.

#### 3.2 Recursive Derivative Estimation and Score-integrand Solver

In score-based exact solution form, the numerical algorithm mainly involves solving the integration of  $\epsilon_{\theta}(\mathbf{x}_t, t)$ . In order to obtain the approximate solution at time 0, an iterative approach is required to solve for each  $\mathbf{x}_t$  along the time trajectory t, as the variable  $\mathbf{x}_t$  in the integrand is only known at time t = T. Given an initial value  $\mathbf{x}_T$  at time t = T and time trajectory  $\{t_i\}_{i=0}^N$ , where  $t_i = T$  and  $t_i = T$  and  $t_i = T$  and time exact solution sequence  $\{\mathbf{x}_t\}_{t=0}^{N-1}$  on time trajectory are given according to Eq. (3.4) by

$$\mathbf{x}_{t_{i-1}} = \frac{\alpha_{t_{i-1}}}{\alpha_{t_i}} \mathbf{x}_{t_i} + \alpha_{t_{i-1}} \int_{\text{NSR}(t_i)}^{\text{NSR}(t_{i-1})} \boldsymbol{\epsilon}_{\theta} \left( \mathbf{x}_{\psi(\tau)}, \psi(\tau) \right) d\tau, \tag{3.5}$$

where  $\mathbf{x}_{t_0}$  is the true solution at time 0,  $\psi(\tau) := \text{rNSR}(\tau)$  for simplicity. Then, by establishing the numerical algorithms, we can iteratively obtain the value at each point along the time trajectory based on Eq. (3.5), and thereby obtain an approximate solution for  $\mathbf{x}_{t_0}$ .

Denote  $h_{t_i} := \text{NSR}(t_{i-1}) - \text{NSR}(t_i)$ ,  $\tau_{t_i} := \text{NSR}(t_i)$ , and  $\epsilon_{\theta}^{(k)} \left( \mathbf{x}_{\psi(\tau)}, \psi(\tau) \right) := \frac{d^k \epsilon_{\theta} \left( \mathbf{x}_{\psi(\tau)}, \psi(\tau) \right)}{d \tau^k}$  as k-th order total derivative of  $\epsilon_{\theta} \left( \mathbf{x}_{\psi(\tau)}, \psi(\tau) \right)$  w.r.t.  $\tau$ . For  $n \ge 1$ , the n-th order Taylor expansion of  $\epsilon_{\theta} \left( \mathbf{x}_{\psi(\tau_{t-1})}, \psi(\tau_{t_{i-1}}) \right)$  w.r.t.  $\tau$  at  $\tau_{t_i}$  is

$$\epsilon_{\theta}\left(\mathbf{x}_{\psi(\tau_{t_{i-1}})}, \psi(\tau_{t_{i-1}})\right) = \sum_{k=0}^{n} \frac{h_{t_{i}}^{k}}{k!} \epsilon_{\theta}^{(k)}\left(\mathbf{x}_{\psi(\tau_{t_{i}})}, \psi(\tau_{t_{i}})\right) + O(h_{t_{i}}^{n+1}). \tag{3.6}$$

By substituting this Taylor expansion into Eq. (3.5), we obtain

$$\mathbf{x}_{t_{i-1}} = \frac{\alpha_{t_{i-1}}}{\alpha_{t_i}} \mathbf{x}_{t_i} + \alpha_{t_{i-1}} \sum_{k=0}^{n} \frac{h_{t_i}^{k+1}}{(k+1)!} \boldsymbol{\epsilon}_{\theta}^{(k)} \left( \mathbf{x}_{\psi(\tau_{t_i})}, \psi(\tau_{t_i}) \right) + O(h_{t_i}^{n+2}). \tag{3.7}$$

Then, we can develop an n-th order solver for diffusion ODEs by omitting the error term  $O(h_{t_i}^{n+1})$  and approximating the first (n-1)-order derivatives  $\epsilon_{\theta}^{(k)}(\mathbf{x}_{\psi(\tau_{t_i})}, \psi(\tau_{t_i}))$  for  $k \leq n-1$  in turn [26]. For example, when n=1, we can obtain the following *first-order iterative algorithm*:

$$\tilde{\mathbf{x}}_{t_{i-1}} = \frac{\alpha_{t_{i-1}}}{\alpha_{t_i}} \tilde{\mathbf{x}}_{t_i} + \alpha_{t_{i-1}} h_i \epsilon_{\theta} \left( \tilde{\mathbf{x}}_{\psi(\tau_{t_i})}, \psi(\tau_{t_i}) \right), \tag{3.8}$$

where  $\tilde{\mathbf{x}}$  is an approximation of the true value  $\mathbf{x}$ , and  $\tilde{\mathbf{x}}_{t_N} = \mathbf{x}_T$  is the given initial value.

However, when dealing with  $n \ge 2$ , evaluating the derivatives requires obtaining additional variables, which are approximate values generated by lower-order algorithms. Therefore, evaluating the derivatives of the score function evaluation directly using conventional finite difference estimation (FDE) methods may present a challenge as errors can propagate easily.

In order to reduce the estimation error introduced by FDE, we propose the recursive derivative estimation (RDE) method for approximating derivatives. This method recursively extracts the required derivative terms at a specific point from the higher-order derivative terms, as shown in Fig 2. Numerical experiments report that replacing the derivative term with the RDE method in the algorithm consistently yields better FID results compared to the FDE method, as shown in Fig. 4. We provide a detailed derivation of the RDE method in Appendix C. Denote  $NSR_{min} := min\{NSR(t_i)\}$ ,  $NSR_{max} := max\{NSR(t_i)\}$ , we have then the following theorem for RDE.

**Theorem 3.1** Let  $\mathbf{x}_s$  be a given initial value at time s > 0,  $\mathbf{x}_t$  be the estimated value at time t obtained by the first-order iterative algorithm in Eq. (3.8). Assume that  $\epsilon_{\theta}(\mathbf{x}_{\psi(\tau)}, \psi(\tau)) \in \mathbb{C}^{\infty}[\mathrm{NSR}_{\min}, \mathrm{NSR}_{\max}]$ . Then, we have

$$\epsilon_{\theta}^{(1)}\left(\tilde{\mathbf{x}}_{\psi(\tau_{s})}, \psi(\tau_{s})\right) = \frac{e}{e-1} \frac{\epsilon_{\theta}\left(\tilde{\mathbf{x}}_{\psi(\tau_{t})}, \psi(\tau_{t})\right) - \epsilon_{\theta}\left(\tilde{\mathbf{x}}_{\psi(\tau_{s})}, \psi(\tau_{s})\right)}{h_{s}} \\
- \frac{\epsilon_{\theta}^{(1)}\left(\tilde{\mathbf{x}}_{\psi(\tau_{t})}, \psi(\tau_{t})\right)}{e-1} - \frac{(e-2)h_{s}}{2(e-1)} \epsilon_{\theta}^{(2)}\left(\tilde{\mathbf{x}}_{\psi(\tau_{t})}, \psi(\tau_{t})\right) + O(h_{s}^{2}), \tag{3.9}$$

where  $\mathbb{C}^{\infty}[NSR_{min}, NSR_{max}]$  denotes  $\epsilon_{\theta}(\mathbf{x}_{\psi(\tau)}, \psi(\tau))$  is an infinitely continuously differentiable function w.r.t.  $\tau$  over the interval [NSR<sub>min</sub>, NSR<sub>max</sub>].

We observe that the differentiability constraint imposed by Theorem 3.1 appears to be rather restrictive. To enhance its broad applicability, we further propose a RDE method with limited differentiability.

**Corollary 1** Let  $\mathbf{x}_s$  be a given initial value at time s > 0,  $\mathbf{x}_t$  be the estimated value at time t obtained by the first-order iterative algorithm in Eq. (3.8). Assume that  $\epsilon_{\theta}(\mathbf{x}_{\psi(\tau)}, \psi(\tau)) \in \mathbb{C}^m[\mathrm{NSR}_{\min}, \mathrm{NSR}_{\max}]$ , i.e., m times continuously differentiable, where  $m \ge 3$ . Then, we have

$$\epsilon_{\theta}^{(1)}\left(\tilde{\mathbf{x}}_{\psi(\tau_{s})}, \psi(\tau_{s})\right) = \frac{1}{\phi_{1}(m)} \frac{\epsilon_{\theta}\left(\tilde{\mathbf{x}}_{\psi(\tau_{t})}, \psi(\tau_{t})\right) - \epsilon_{\theta}\left(\tilde{\mathbf{x}}_{\psi(\tau_{s})}, \psi(\tau_{s})\right)}{h_{s}} \\
- \frac{\phi_{2}(m)}{\phi_{1}(m)} \epsilon_{\theta}^{(1)}\left(\tilde{\mathbf{x}}_{\psi(\tau_{t})}, \psi(\tau_{t})\right) - \frac{\phi_{3}(m)h_{s}}{\phi_{1}(m)} \epsilon_{\theta}^{(2)}\left(\tilde{\mathbf{x}}_{\psi(\tau_{t})}, \psi(\tau_{t})\right) + O(h_{s}^{2}), \tag{3.10}$$

where 
$$\phi_1(m) = \sum_{k=1}^m \frac{(-1)^{k-1}}{k!}$$
,  $\phi_2(m) = \sum_{k=2}^m \frac{(-1)^k}{k!}$ , and  $\phi_3(m) = \sum_{k=3}^m \frac{(-1)^{k+1}}{k!}$ .

The proofs of Theorem 3.1 and Corollary 1 are in Appendix C. As high-order algorithms are generally more sensitive to numerical errors, we consider truncating the Taylor expansion to at most three terms, and leaving the handling of the case  $k \ge 4$  for future study. Based on the Eq. (3.7) and the RDE method stated by Corollary 1 and Theorem 3.1, we propose two algorithms named SciRE-Solver-2 and SciRE-Solver-3 for n = 2 and n = 3, respectively.

Under mild assumptions, we prove that the SciRE-Solver-k (k = 2, 3) is a kth-order solver, as stated in the following theorem. The proof is given in Appendix D.

**Theorem 3.2** Assume that  $\epsilon_{\theta}(\mathbf{x}_{\psi(\tau)}, \psi(\tau)) \in \mathbb{C}^m[\mathrm{NSR}_{\min}, \mathrm{NSR}_{\max}]$ . Then, for k=2,3, the global convergence order of SciRE-Solver-k is no less than k-1.

#### Algorithm 1 SciRE-Solver-2

**Require:** initial value  $\mathbf{x}_T$ , time trajectory  $\{t_i\}_{i=0}^N$ , model  $\epsilon_{\theta}, m \geq 3$ 

- 1:  $\tilde{\mathbf{x}}_{t_N} \leftarrow \mathbf{x}_T, r_1 \leftarrow \frac{1}{2}$ 2: **for**  $i \leftarrow N$  to 0 **do**
- $h_i \leftarrow \text{NSR}(t_{i-1}) \text{NSR}(t_i)$

- $s_{i} \leftarrow \text{rNSR}\left(\text{NSR}(t_{i}) + r_{1}h_{i}\right)$   $\tilde{\mathbf{x}}_{s_{i}} \leftarrow \frac{\alpha_{s_{i}}}{\alpha_{t_{i}}}\tilde{\mathbf{x}}_{t_{i}} + \alpha_{s_{i}}r_{1}h_{i}\boldsymbol{\epsilon}_{\theta}\left(\tilde{\mathbf{x}}_{t_{i}}, t_{i}\right)$   $\tilde{\mathbf{x}}_{t_{i-1}} \leftarrow \frac{\alpha_{t_{i-1}}}{\alpha_{t_{i}}}\tilde{\mathbf{x}}_{t_{i}} + \alpha_{t_{i-1}}h_{i}\boldsymbol{\epsilon}_{\theta}\left(\tilde{\mathbf{x}}_{t_{i}}, t_{i}\right) + \alpha_{t_{i-1}}\frac{h_{i}}{2\phi_{1}(m)r_{1}}\left(\boldsymbol{\epsilon}_{\theta}\left(\tilde{\mathbf{x}}_{s_{i}}, s_{i}\right) \boldsymbol{\epsilon}_{\theta}\left(\tilde{\mathbf{x}}_{t_{i}}, t_{i}\right)\right)$
- 7: end for

**Return:**  $\tilde{\mathbf{x}}_0$ .

### Algorithm 2 SciRE-Solver-3

```
Require: initial value \mathbf{x}_{T}, time trajectory \{t_{i}\}_{i=0}^{N}, model \boldsymbol{\epsilon}_{\theta}, m \geq 3

1: \tilde{\mathbf{x}}_{t_{N}} \leftarrow \mathbf{x}_{T}, r_{1} \leftarrow \frac{1}{3}, r_{2} \leftarrow \frac{2}{3}

2: for i \leftarrow N to 0 do

3: h_{i} \leftarrow \text{NSR}(t_{i-1}) - \text{NSR}(t_{i})

4: s_{i_{1}}, s_{i_{2}} \leftarrow \text{rNSR}(\text{NSR}(t_{i}) + r_{1}h_{i}), rNSR (NSR(t_{i}) + r_{2}h_{i})

5: \mathbf{x}_{s_{i_{1}}} \leftarrow \frac{\alpha_{s_{i_{1}}}}{\alpha_{t_{i}}} \mathbf{x}_{t_{i}} + \alpha_{s_{i_{1}}} r_{1}h_{i}\boldsymbol{\epsilon}_{\theta}(\mathbf{x}_{t_{i}}, t_{i})

6: \mathbf{x}_{s_{i_{2}}} \leftarrow \frac{\alpha_{s_{i_{2}}}}{\alpha_{t_{i}}} \mathbf{x}_{t_{i}} + \alpha_{s_{i_{2}}} r_{2}h_{i}\boldsymbol{\epsilon}_{\theta}(\mathbf{x}_{t_{i}}, t_{i}) + \alpha_{s_{i_{2}}} \frac{h_{i}}{\phi_{1}(m)} \left(\boldsymbol{\epsilon}_{\theta}\left(\mathbf{x}_{s_{i_{1}}}, s_{i_{1}}\right) - \boldsymbol{\epsilon}_{\theta}\left(\mathbf{x}_{t_{i}}, t_{i}\right)\right)

7: \mathbf{x}_{t_{i-1}} \leftarrow \frac{\alpha_{t_{i-1}}}{\alpha_{t_{i}}} \mathbf{x}_{t_{i}} + \alpha_{t_{i-1}}h_{i}\boldsymbol{\epsilon}_{\theta}(\mathbf{x}_{t_{i}}, t_{i}) + \alpha_{t_{i-1}} \frac{h_{i}}{2\phi_{1}(m)r_{2}} \left(\boldsymbol{\epsilon}_{\theta}\left(\mathbf{x}_{s_{i_{2}}}, s_{i_{2}}\right) - \boldsymbol{\epsilon}_{\theta}(\mathbf{x}_{t_{i}}, t_{i})\right)

8: end for

Return: \mathbf{x}_{0}.
```

#### 3.3 Parametrizable Time Trajectory

In SciRE-Solver, it is necessary to specify a time trajectory. Although SciRE-Solver can generate high-quality samples in just a few steps using existing quadratic and uniform time trajectories as shown in Appendix E, it has been demonstrated in experiments in [13] and [28] that the optimal time trajectory can further improve the sampling efficiency. Therefore, we further propose two parametrized alternative methods for the NSR function to compute the time trajectory, respectively, named as NSR-type and Sigmoid-type time trajectories. Therefore, we propose two parameterized alternative method for computing the time trajectory of NSR function, named the NSR-type and Sigmoid-type trajectories, respectively. The comparative experiments are provided in Appendix E.

#### 3.4 Algorithms Comparison and Different Exact Solution Forms for Diffusion ODE

In fact, the first-order algorithm given in Eq. (3.8) is completely identical to DDIM [14], so we do not include it in our SciRE-Solver. Next, we show that our SciRE-Solver differs fundamentally from the DPM-Solver[13]. In [13], DPM-Solver provided the following solution form for the diffusion ODE:

$$\mathbf{x}_{t} = \frac{\alpha_{t}}{\alpha_{s}} \mathbf{x}_{s} - \alpha_{t} \int_{\lambda_{s}}^{\lambda_{t}} e^{-\lambda} \hat{\boldsymbol{\epsilon}}_{\theta} \left( \hat{\mathbf{x}}_{\lambda}, \lambda \right) d\lambda$$
 (3.11)

where  $\lambda_t = \log \frac{\alpha_t}{\sigma_t}$ ,  $\hat{\epsilon}_{\theta}(\hat{\mathbf{x}}_{\lambda}, \lambda) = \epsilon_{\theta}(\mathbf{x}_{t(\lambda)}, t(\lambda))$ , and  $t(\lambda)$  is the inverse function of  $\lambda_t$  w.r.t. time t. We observe that the score-based solution form in Eq. (3.4) can be transformed into the solution form provided by the DPM-Solver in Eq. (3.11) by making a change-of-variable  $\tau = e^{-\lambda}$ . However, different forms of exact solutions result in different integrands and distinct Taylor series expansions, thereby guiding distinct numerical algorithms. One of the most notable examples is when dealing with stiff ODEs, where changes-of-variable are often employed to enhance the performance of numerical algorithms. Specifically, we expand  $\epsilon_{\theta}(\mathbf{x}_{\psi(\tau)}, \psi(\tau))$  in a Taylor series around  $\tau$ , which is distinct from DPM-Solver where  $\epsilon_{\theta}(\mathbf{x}_{t(\lambda)}, t(\lambda))$  is expanded w.r.t.  $\lambda$ , as  $\tau \neq \lambda$ . Conducting distinct Taylor expansions under different forms of exact solutions results in further variations of the integrands. For example, the integrand in our case does not exhibit prominent exponential characteristics as observed in DPM-Solver. Moreover, SciRE-Solver, derived from our proposed RDE method, distinguishes itself significantly from DPM-Solver [13] and fast sampling algorithms in literature such as [24, 28, 25]. Finally, due to the fact that other exact solution forms of the diffusion ODE can be obtained by using different changes-of-variable on our exact solution form in Eq. (3.4), we have the following remark.

**Remark 1** An optimal transformation may exist to guide the development of the optimal numerical solver for the diffusion ODE by obtaining an appropriate exact solution form.

## 4 Experiments

In this section, we show that SciRE-Solver can significantly improve the sampling efficiency of pretrained DPM models, including continuous-time and discrete-time DPMs. Specifically, we conduct sampling experiments using individual SciRE-Solver-2 and SciRE-Solver-3 on the pre-trained models of the diffusion model. For each experiments, we draw 50K samples and assess sample quality using the widely adopted FID score [32], where lower FID generally indicate better sample quality. In order to facilitate the exploration of more possibilities of the SciRE-Solver our proposed and to fully utilize the given number of score function evaluations (NFE), we defined a simple combinatorial version based on SciRE-Solver-*k* and named as SciRE-Solver-agile, as detailed in Appendix E. When comparing with other existing fast sampling algorithms, we will compare the best FID values reported by these algorithms in the relevant literature with the FID obtained by our proposed SciRE-Solver under the same NFE, as shown in Table 1. Meanwhile, we evaluated the generative performance of DDIM, DPM-Solver, and SciRE-Solver on CIFAR-10 and CelebA 64×64 datasets with the same time trajectories, settings and codebase, the corresponding numerical results are reported in Table 2.

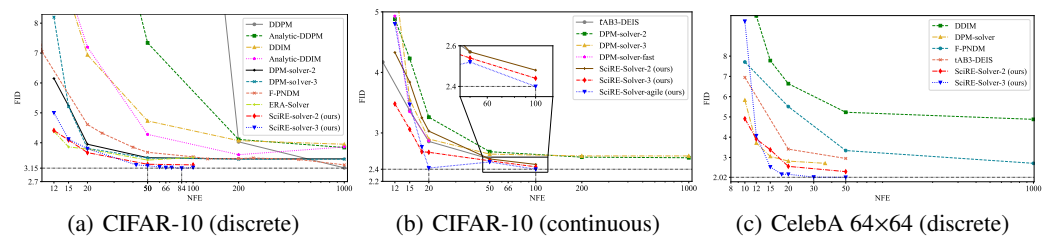


Figure 3: The comparative diagram of FID  $\downarrow$  of different training-free sampling methods on the CIFAR-10 and CelebA 64×64 datasets. In these three cases, our samplers reach SOTA.

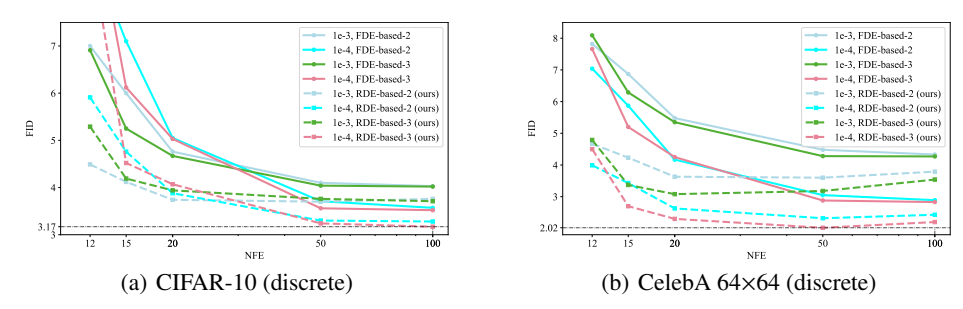


Figure 4: Comparison of FID ↓ obtained by employing RDE and FDE in SciRE-Solver codebase.

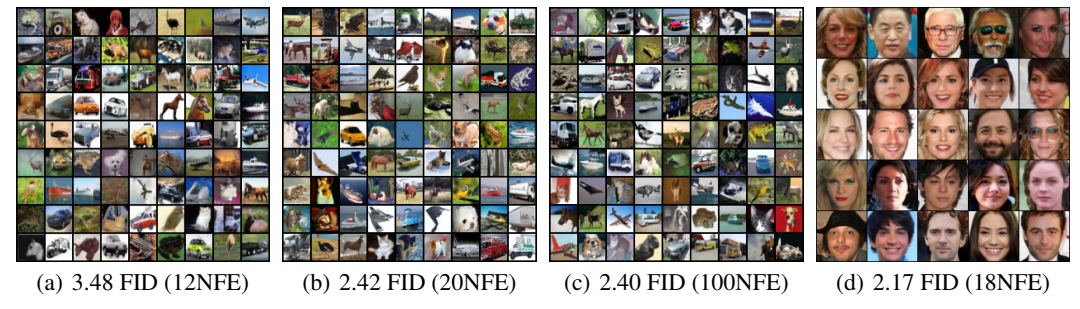


Figure 5: Samples generated by SciRE-Solver on CIFAR-10 and CelebA 64×64 datasets.

## 4.1 Experiment Setting and Ablation Study

When running our proposed SciRE-Solver-k in Algorithms 1 and 2, it is necessary to assign a value m to  $\phi_1(m)$ . As stated in Corollary 1, when assigning m, we need to ensure that  $m \ge 3$ . Considering that the limit of  $\phi_1(m)$  is  $\frac{e-1}{e}$ , then our experiments only consider these two extreme cases, i.e., we only choose to allocate m as 3 or directly set  $\phi_1(m) = \frac{e-1}{e}$ . We provide ablation experiments for these two cases in Appendix E. Moreover, in Appendix E, we also conducted ablation experiments on different types of time trajectories (uniform, quadratic, logSNR, and we proposed NSR and Sigmoid), different sampling endpoints (1e-3) and (1e-4), and different (1e-3) and (1e-4), and different (1e-3) and (1e-4), and different (1e-3) and (1e-4). All our experiments are run on TITAN-V GPU.

## 4.2 Comparison between the Using of RDE Method and Non-RDE

In Corollary 1, if we set  $\phi_1(m) = 1$  and drop other terms, the RDE method degenerates into the finite difference estimation (*FDE*) method. Thus, we set  $\phi_1(m) = 1$  in our SciRE-Solver codebase

to represent the sampling algorithm based on FDE. Numerical experimental report that, under the same codebase and settings, the quality of samples obtained by SciRE-Solver with RDE method is consistently superior to of samples obtained by the Solver with FDE method, as shown in Fig 4.

## 4.3 Comparison with Discrete-Time Sampling Methods

We compare SciRE-Solver proposed in Section 3.2 with existing discrete-time training-free methods, including DDPM [2], DDIM [14], Analytic-DDPM and Analytic-DDIM [33], PNDM [24], DPM-Solver [13], DEIS [28], and ERA-Solver [25]. Specifically, we use the discrete-time model trained by  $L_{\text{simple}}$  in [2] on CIFAR-10 and CelebA 64×64 datasets with linear noise schedule, and assign m=3 to  $\phi_1(m)$ . Under this setting, we use the same NSR-type time trajectory with fixed parameter for both SciRE-Solver-2 and SciRE-Solver-3, the details are available in Appendix E. Experimental results demonstrate that SciRE-solver achieves higher sample quality compared to other samplers in an efficient manner, as shown in (a) and (c) of Fig 3. Meanwhile, SciRE-solver almost reaches convergence at around 66 NFE and 18 NFE, achieving the new state-of-the-art (SOTA) values of 3.15 FID with 84 NFE, and of 2.17 FID with 18 NFE on CIFAR-10 and CelebA 64×64, respectively. Table 1 displays the specific FID scores obtained by different samplers with varying NFEs.

#### 4.4 Comparison with Continuous-Time Sampling Methods

We compare SciRE-Solver-k and SciRE-Solver-agile with DPM-Solver-k [13], DPM-Solver-fast and DEIS [28], where k=2, 3. On CIFAR-10, we use "VP deep" model [3] with the linear noise schedule. When NFE  $\geq$  15, we employ the identical NSR-type time trajectories with consistent parametric functions for SciRE-Solver-2 and SciRE-Solver-3, respectively, the details are available in Appendix E. Meanwhile, we consider using the sigmoid-type time trajectory only when NFE is less than 15. The superior performance of SciRE-Solver is particularly evident in its ability to generate high-quality samples with 2.42 FID in just 20 NFE, as shown in (b) of Fig 3. Furthermore, supported by several experimental validations, SciRE-Solver achieves 2.40 FID in just 100 NFE, which attains a new state-of-the-art (SOTA) generative capability under the VP-deep model [3] that we used. Table 1 displays the specific FID scores obtained by different samplers at varying NFEs.

#### 5 Conclusions

In this work, from the perspective of we derived exact solution form of diffusion ODEs, we propose SciRE-Solver, an efficient specialized solver with training-free, to tackle the problem of efficient sampling from DPMs. In SciRE-Solver, to reduce numerical estimation errors, we introduce an RDE method for estimating the derivatives of the score function evaluation in DPMs. We also propose two parametrizable time trajectory, named NSR-type and Sigmoid-type time trajectories. Numerical experiments report that SciRE-Solver not only can efficiently generates high-quality samples on different datasets with the few-step sampling regime, but also demonstrates the potential to surpass the FID shown in the original papers of some pre-trained models.

**Limitations and broader impact** SciRE-Solver has demonstrated the ability to surpass the FID scores shown in the original papers of some pre-trained models on CIFAR-10 and CelebA 64×64 datasets with a small NFEs. This indicates that developing efficient sampling algorithms can further enhance the generative capacity of existing pre-trained models. However, for fast sampling, it is a open question whether there exists an optimal time trajectory for SciRE-Solver and other fast samplers. Moreover, fast sampling algorithms may overly rely on local information during the acceleration process, resulting in excessive noise or bias.

## Acknowledgments

The first author is very grateful for the valuable feedback received from the authors of the DPM-Solver paper during the early stage of this work regarding program-related issues. This work was supported in part by grants from National Science Foundation of China (61571005), the fundamental research program of Guangdong, China (2020B1515310023,2023A1515011281).

## References

[1] Sohl-Dickstein, J., Weiss, E., Maheswaranathan, N., Ganguli, S.: Deep unsupervised learning using nonequilibrium thermodynamics. In: International Conference on Machine Learning, PMLR (2015) 2256–2265

Sampling method \NFE	12	15	20	50	200	1000			
CIFAR-10 (discrete-time m	odel [2],	linear no	ise sched	lule)					
DDPM [2]	246.3	197.6	137.3	32.6	4.03	3.16			
Analytic-DDPM [33]	27.69	20.82	15.35	7.34	4.11	3.84			
DDIM [14]	11.02	8.92	6.94	4.73	4.07	3.95			
Analytic-DDIM [33]	11.68	9.16	7.20	4.28	3.60	3.86			
tAB3-DEIS [28]	7.12(10	NFE)	4.53	3.78	\	\			
DPM-Solver-2 [13]	6.15	†5.23	3.95	3.50	3.46	3.46			
DPM-Solver-3 [13]	8.20	5.21	†3.81	†3.49	†3.45	†3.45			
F-PNDM [24]	7.03(10	NFE)	4.61	3.68	3.47	3.26			
ERA-Solver [25]	4.38	3.86	3.79	3.42	3.51(	100NFE)			
SciRE-Solver-2 (ours)	4.41	†4.09	3.67	3.28	3.26(	100NFE)			
SciRE-Solver-3 (ours)	5.00	4.12	†3.80	†3.23	3.15	(84NFE)			
CIFAR-10 (VP deep contin	uous-tim	e model	[3])						
DPM-Solver-2 [13]	4.88	†4.23	3.26	2.69	2.60	2.59			
DPM-Solver-3 [13]	5.53	3.55	†2.90	†2.65	†2.62	†2.62			
DPM-Solver-fast [13]	4.93	3.35	2.87	\	\	\			
tAB3-DEIS [28]	\	3.37	2.86	2.57	\	\			
SciRE-Solver-2 (ours)	4.33	†3.84	3.03	2.57		100NFE)			
SciRE-Solver-3 (ours)	3.48	3.06	†2.68	†2.54		(100NFE)			
SciRE-Solver-agile (ours)	4.80	3.47	2.42	2.52	2.40 (	100NFE)			
CelebA 64×64 (discrete-tin	CelebA 64×64 (discrete-time model [14], linear noise schedule)								
Sampling method \NFE	10	12	15	20	50	1000			
DDIM [14]	10.85	9.99	7.78	6.64	5.23	4.88			
DPM-Solver [13]	5.83	3.71	3.05	2.82	2.71	(36NFE)			
F-PNDM [24]	7.71	\	\	5.51	3.34	2.71			
tAB3-DEIS [28]	6.95	\	\	3.41	2.95	\			
SciRE-Solver-2 (ours)	4.91	3.91	†3.38	2.56	2.30	_			
SciRE-Solver-3 (ours)	†9.72	4.07	2.53	† <b>2.17</b>	<sup>†</sup> 2.02	_			

Table 1: Generation quality measured by FID | of different sampling methods for DPMs on CIFAR-10 and CelebA 64×64 with discrete-time continuous-time pre-training models. In this Table, we compare the best FID reported in existing literature with the FID achieved by our proposed SciRE-Solver at the same NFE. The bold black represents the best result obtained under the same NFE (column). The results with † means the actual NFE is smaller than the given NFE because the given NFE cannot be divided by 2 or 3. Some results are missing in their original papers, which are replaced by " Here, we used the same time trajectory scheme to evaluate the results of SciRE-Solver on CIFAR-10 and CelebA 64×64 datasets with discrete models. setting of continuoustime on CIFAR-10 are described in Section 4.4. More comparisons and additional details are shown in Appendix E.

- [2] Ho, J., Jain, A., Abbeel, P.: Denoising diffusion probabilistic models. Advances in Neural Information Processing Systems **33** (2020) 6840–6851
- [3] Song, Y., Sohl-Dickstein, J., Kingma, D.P., Kumar, A., Ermon, S., Poole, B.: Score-based generative modeling through stochastic differential equations. In: International Conference on Learning Representations. (2021)
- [4] Dhariwal, P., Nichol, A.: Diffusion models beat gans on image synthesis. Advances in Neural Information Processing Systems **34** (2021) 8780–8794
- [5] Meng, C., He, Y., Song, Y., Song, J., Wu, J., Zhu, J.Y., Ermon, S.: SDEdit: Guided image synthesis and editing with stochastic differential equations. In: International Conference on Learning Representations. (2022)
- [6] Ramesh, A., Dhariwal, P., Nichol, A., Chu, C., Chen, M.: Hierarchical text-conditional image generation with clip latents. arXiv preprint arXiv:2204.06125 (2022)
- [7] Ho, J., Chan, W., Saharia, C., Whang, J., Gao, R., Gritsenko, A., Kingma, D.P., Poole, B., Norouzi, M., Fleet, D.J., et al.: Imagen video: High definition video generation with diffusion models. arXiv preprint arXiv:2210.02303 (2022)
- [8] Chen, N., Zhang, Y., Zen, H., Weiss, R.J., Norouzi, M., Chan, W.: Wavegrad: Estimating gradients for waveform generation. In: International Conference on Learning Representations. (2021)
- [9] Liu, J., Li, C., Ren, Y., Chen, F., Zhao, Z.: Diffsinger: Singing voice synthesis via shallow diffusion mechanism. In: Proceedings of the AAAI Conference on Artificial Intelligence. Volume 36. (2022) 11020–11028

- [10] Goodfellow, I., Pouget-Abadie, J., Mirza, M., Xu, B., Warde-Farley, D., Ozair, S., Courville, A., Bengio, Y.: Generative adversarial networks. Communications of the ACM 63(11) (2020) 139–144
- [11] Kingma, D.P., Welling, M.: Auto-encoding variational bayes. arXiv preprint arXiv:1312.6114 (2013)
- [12] Chen, R.T., Rubanova, Y., Bettencourt, J., Duvenaud, D.K.: Neural ordinary differential equations. Advances in neural information processing systems **31** (2018)
- [13] Lu, C., Zhou, Y., Bao, F., Chen, J., Li, C., Zhu, J.: Dpm-solver: A fast ode solver for diffusion probabilistic model sampling in around 10 steps. Advances in Neural Information Processing Systems (2022)
- [14] Song, J., Meng, C., Ermon, S.: Denoising diffusion implicit models. In: International Conference on Learning Representations. (2021)
- [15] Salimans, T., Ho, J.: Progressive distillation for fast sampling of diffusion models. In: International Conference on Learning Representations. (2021)
- [16] Meng, C., Rombach, R., Gao, R., Kingma, D., Ermon, S., Ho, J., Salimans, T.: On distillation of guided diffusion models. In: Proceedings of the IEEE/CVF Conference on Computer Vision and Pattern Recognition. (2023) 14297–14306
- [17] Luo, W.: A comprehensive survey on knowledge distillation of diffusion models. arXiv preprint arXiv:2304.04262 (2023)
- [18] Song, Y., Dhariwal, P., Chen, M., Sutskever, I.: Consistency models. arXiv preprint arXiv:2303.01469 (2023)
- [19] Nichol, A.Q., Dhariwal, P.: Improved denoising diffusion probabilistic models. In: International Conference on Machine Learning, PMLR (2021) 8162–8171
- [20] Watson, D., Chan, W., Ho, J., Norouzi, M.: Learning fast samplers for diffusion models by differentiating through sample quality. In: International Conference on Learning Representations. (2022)
- [21] Xiao, Z., Kreis, K., Vahdat, A.: Tackling the generative learning trilemma with denoising diffusion GANs. In: International Conference on Learning Representations. (2022)
- [22] Vahdat, A., Kreis, K., Kautz, J.: Score-based generative modeling in latent space. Advances in Neural Information Processing Systems **34** (2021) 11287–11302
- [23] Zhang, Q., Chen, Y.: Diffusion normalizing flow. Advances in Neural Information Processing Systems 34 (2021) 16280–16291
- [24] Liu, L., Ren, Y., Lin, Z., Zhao, Z.: Pseudo numerical methods for diffusion models on manifolds. In: International Conference on Learning Representations. (2022)
- [25] Li, S., Liu, L., Chai, Z., Li, R., Tan, X.: Era-solver: Error-robust adams solver for fast sampling of diffusion probabilistic models. arXiv preprint arXiv:2301.12935 (2023)
- [26] Atkinson, K., Han, W., Stewart, D.E.: Numerical solution of ordinary differential equations. John Wiley & Sons (2011)
- [27] Mohazzabi, P., Becker, J.L.: Numerical solution of differential equations by direct taylor expansion. Journal of Applied Mathematics and Physics 5(3) (2017) 623–630
- [28] Zhang, Q., Chen, Y.: Fast sampling of diffusion models with exponential integrator. In: The Eleventh International Conference on Learning Representations. (2023)
- [29] Kingma, D., Salimans, T., Poole, B., Ho, J.: Variational diffusion models. Advances in neural information processing systems 34 (2021) 21696–21707

- [30] Dormand, J.R., Prince, P.J.: A family of embedded runge-kutta formulae. Journal of computational and applied mathematics **6**(1) (1980) 19–26
- [31] Hale, J.K., Lunel, S.M.V.: Introduction to functional differential equations. Volume 99. Springer Science & Business Media (2013)
- [32] Heusel, M., Ramsauer, H., Unterthiner, T., Nessler, B., Hochreiter, S.: Gans trained by a two time-scale update rule converge to a local nash equilibrium. Advances in neural information processing systems **30** (2017)
- [33] Bao, F., Li, C., Zhu, J., Zhang, B.: Analytic-DPM: an analytic estimate of the optimal reverse variance in diffusion probabilistic models. In: International Conference on Learning Representations. (2022)
- [34] Rombach, R., Blattmann, A., Lorenz, D., Esser, P., Ommer, B.: High-resolution image synthesis with latent diffusion models (2021)
- [35] Lu, C., Zhou, Y., Bao, F., Chen, J., Li, C., Zhu, J.: Dpm-solver++: Fast solver for guided sampling of diffusion probabilistic models. arXiv preprint arXiv:2211.01095 (2022)

## Appendix A Diffusion SDEs, Diffusion ODEs and SciRE-Solver

#### A.1 Diffusion SDEs

In the forward diffusion process of DPMs for *D*-dimensional data, a Markov sequence  $\{\mathbf{x}_t\}_{t \in [0,T]}$  with T > 0 starting with  $\mathbf{x}_0$  is defined by the transition distribution

$$q(\mathbf{x}_t \mid \mathbf{x}_{t-1}) := \mathcal{N}\left(\mathbf{x}_t; \beta_t \mathbf{x}_{t-1}, \left(1 - \beta_t^2\right) \mathbf{I}\right), \tag{A.1}$$

where  $\beta_t \in \mathbb{R}^+$  is the variance schedule function. With the transition distribution in Eq. (2.1), one can formulate the transition kernel of noisy data  $\mathbf{x}_t$  conditioned on clean data  $\mathbf{x}_0$  as

$$q(\mathbf{x}_t \mid \mathbf{x}_0) = \mathcal{N}(\mathbf{x}_t; \alpha_t \mathbf{x}_0, \sigma_t^2 \mathbf{I}), \tag{A.2}$$

where  $\alpha_t = \prod_{i=1}^t \beta_i$ ,  $\sigma_t = \sqrt{1 - \alpha_t^2}$  for the variance-preserving setting. Clearly,  $\alpha_t$ ,  $\sigma_t \in \mathbb{R}^+$  are also differentiable function of time t with bounded derivatives like  $\beta_t$ .  $\alpha_t^2/\sigma_t^2$  is strictly decreasing w.r.t. t, and called the signal-to-noise-ratio (SNR) in [29]. In [29], Kingma et al. established the equivalence between the transition kernel of the following SDE and the one in Eq. (A.2) for  $\forall t \in [0, T]$ :

$$d\mathbf{x}_{t} = f(t)\mathbf{x}_{t} dt + g(t)d\omega_{t}, \quad \mathbf{x}_{0} \sim q_{0}(\mathbf{x}_{0}), \tag{A.3}$$

where  $\omega_t \in \mathbb{R}^D$  denotes a standard Wiener process, and

$$f(t) = \frac{\mathrm{d}\log\alpha_t}{\mathrm{d}t}, \quad g^2(t) = \frac{\mathrm{d}\sigma_t^2}{\mathrm{d}t} - 2\frac{\mathrm{d}\log\alpha_t}{\mathrm{d}t}\sigma_t^2. \tag{A.4}$$

Further, Song et al. [3] demonstrated with some regularity conditions that the forward process in Eq. (A.2) has the following equivalent reverse process (*reverse SDE*) from time T to 0:

$$d\mathbf{x}_{t} = \left[ f(t)\mathbf{x}_{t} - g^{2}(t)\nabla_{\mathbf{x}}\log q_{t}(\mathbf{x}_{t}) \right] dt + g(t)d\overline{\omega}_{t}, \quad \mathbf{x}_{T} \sim q_{T}(\mathbf{x}_{T}), \tag{A.5}$$

where  $\overline{\omega}_t$  represents a standard Wiener process in the reverse time. Since f(t) and g(t) are determined by the noise schedule  $(\alpha_t, \sigma_t)$  in the reverse SDE (A.5), the sole term that remains unknown is the score function  $\nabla_{\mathbf{x}} \log q_t(\mathbf{x}_t)$  at each time t. Therefore, DPMs train the model by using a neural network  $\epsilon_{\theta}(\mathbf{x}_t, t)$  parameterized by  $\theta$  to approximate the scaled score function:  $-\sigma_t \nabla_{\mathbf{x}} \log q_t(\mathbf{x}_t)$ , where the parameter  $\theta$  is trained by a re-weighted variant of the evidence lower bound (ELBO) [2, 3]:

$$\mathcal{L}(\theta; \lambda(t)) = \frac{1}{2} \int_{0}^{T} \lambda(t) \mathbb{E}_{q_{t}(\mathbf{x}_{t})} \left[ \left\| \boldsymbol{\epsilon}_{\theta} \left( \mathbf{x}_{t}, t \right) + \sigma_{t} \nabla_{\mathbf{x}} \log q_{t} \left( \mathbf{x}_{t} \right) \right\|_{2}^{2} \right] dt$$

$$= \frac{1}{2} \int_{0}^{T} \lambda(t) \mathbb{E}_{q_{0}(\mathbf{x}_{0})} \mathbb{E}_{q(\epsilon)} \left[ \left\| \boldsymbol{\epsilon}_{\theta} \left( \mathbf{x}_{t}, t \right) - \boldsymbol{\epsilon} \right\|_{2}^{2} \right] dt + C,$$
(A.6)

where  $\epsilon \sim q(\epsilon) = \mathcal{N}(\epsilon; \mathbf{0}, \mathbf{I}), \mathbf{x}_t = \alpha_t \mathbf{x}_0 + \sigma_t \epsilon$ ,  $\lambda(t)$  represents a weighting function, and C is a  $\theta$ -independent constant. After the model is trained, DPMs replace the score function in Eq. (A.3) with  $-\epsilon_{\theta}(\mathbf{x}_t, t) / \sigma_t$  and define the following diffusion SDE:

$$d\mathbf{x}_{t} = \left[ f(t)\mathbf{x}_{t} + \frac{g^{2}(t)}{\sigma_{t}} \boldsymbol{\epsilon}_{\theta} \left( \mathbf{x}_{t}, t \right) \right] dt + g(t) d\overline{\omega}_{t}, \quad \mathbf{x}_{T} \sim \mathcal{N} \left( \mathbf{0}, \hat{\sigma}^{2} \boldsymbol{I} \right). \tag{A.7}$$

DPMs can generate samples by numerically solving the diffusion SDE stated in Eq. (A.7) using discretization methods that span from T to 0.

#### A.2 Diffusion ODEs

Based on the reverse SDE in Eq. (A.5), Song et al. [3] derived a Liouville equation by investigating the evolution equation (Fokker-Planck Equation) of the probability density function of the variable  $\mathbf{x}_t$ . This Liouville equation has the same probability density function w.r.t. the variable  $\mathbf{x}_t$  as that of the reverse SDE. As a result, the reverse SDE can be transformed into the following ODE:

$$\frac{\mathrm{d}\mathbf{x}_{t}}{\mathrm{d}t} = f(t)\mathbf{x}_{t} - \frac{1}{2}g^{2}(t)\nabla_{\mathbf{x}}\log q_{t}\left(\mathbf{x}_{t}\right), \quad \mathbf{x}_{T} \sim q_{T}\left(\mathbf{x}_{T}\right),\tag{A.8}$$

where  $\mathbf{x}_t$  has a marginal distribution  $q_t(\mathbf{x}_t)$ , which is equivalent to the marginal distribution of  $\mathbf{x}_t$  of the reverse SDE in Eq. (A.5). Since the  $\epsilon_{\theta}(\mathbf{x}_t, t)$  trained in Eq. (A.6) can also be thought of as predicting the Gaussian noise added to  $\mathbf{x}_t$ , it is commonly referred to as the *noise prediction model*. By substituting the trained noise prediction model for the score function in Eq. (A.8), Song et al. [3] defined the following *diffusion ODE* for DPMs:

$$\frac{\mathrm{d}\mathbf{x}_{t}}{\mathrm{d}t} = f(t)\mathbf{x}_{t} + \frac{g^{2}(t)}{2\sigma_{t}}\boldsymbol{\epsilon}_{\theta}\left(\mathbf{x}_{t}, t\right), \quad \mathbf{x}_{T} \sim \mathcal{N}\left(\mathbf{0}, \hat{\sigma}^{2} \boldsymbol{I}\right). \tag{A.9}$$

Therefore, one can also generate samples by solving the diffusion ODE from T to 0.

#### A.3 Algorithms of SciRE-Solver

In Section 3.2, we propose the *recursive derivative estimation* (RDE) method for approximating derivatives, the conclusion as shown in Theorem 3.1 and Corollary 1. In this section, we discuss in detail the SciRE-Solver based on RDE.

We review that the *n*-th order Taylor expansion of  $\epsilon_{\theta}(\mathbf{x}_{\psi(\tau_s)}, \psi(\tau_s))$  w.r.t.  $\tau$  at  $\tau_t$  is

$$\boldsymbol{\epsilon}_{\theta} \left( \mathbf{x}_{\psi(\tau_s)}, \psi(\tau_s) \right) = \sum_{k=0}^{n} \frac{h_t^k}{k!} \boldsymbol{\epsilon}_{\theta}^{(k)} \left( \mathbf{x}_{\psi(\tau_t)}, \psi(\tau_t) \right) + O(h_t^{n+1}). \tag{A.10}$$

After substituting this Taylor expansion into Eq. (3.5), we obtain

$$\mathbf{x}_s = \frac{\alpha_s}{\alpha_t} \mathbf{x}_t + \alpha_s \sum_{k=0}^n \frac{h_t^{k+1}}{(k+1)!} \boldsymbol{\epsilon}_{\theta}^{(k)} \left( \mathbf{x}_{\psi(\tau_t)}, \psi(\tau_t) \right) + O(h_t^{n+2}). \tag{A.11}$$

When n = 2, we have then the following truncation formula:

$$\tilde{\mathbf{x}}_{s} = \frac{\alpha_{s}}{\alpha_{t}} \mathbf{x}_{t} + \alpha_{s} \left( h_{t} \boldsymbol{\epsilon}_{\theta}(\mathbf{x}_{\psi(\tau_{t})}, \psi(\tau_{t})) + \frac{h_{t}^{2}}{2} \boldsymbol{\epsilon}_{\theta}^{(1)}(\mathbf{x}_{\psi(\tau_{t})}, \psi(\tau_{t})) + \frac{h_{t}^{3}}{6} \boldsymbol{\epsilon}_{\theta}^{(2)}(\mathbf{x}_{\psi(\tau_{t})}, \psi(\tau_{t})) + O(h_{t}^{4}) \right), \quad (A.12)$$

where  $\tilde{\mathbf{x}}_s$  represents the approximate value of  $\mathbf{x}_s$ . By the RDE method in Corollary 1, we have

$$\boldsymbol{\epsilon}_{\theta}^{(1)}\left(\mathbf{x}_{\psi(\tau_{t})}, \psi(\tau_{t})\right) = \frac{1}{\phi_{1}(m)} \frac{\boldsymbol{\epsilon}_{\theta}\left(\tilde{\mathbf{x}}_{\psi(\tau_{s1})}, \psi(\tau_{s1})\right) - \boldsymbol{\epsilon}_{\theta}\left(\mathbf{x}_{\psi(\tau_{t})}, \psi(\tau_{t})\right)}{r_{1}h_{t}} \\
- \frac{\phi_{2}(m)}{\phi_{1}(m)} \boldsymbol{\epsilon}_{\theta}^{(1)}\left(\mathbf{x}_{\psi(\tau_{s1})}, \psi(\tau_{s1})\right) - \frac{\phi_{3}(m)r_{1}h_{t}}{\phi_{1}(m)} \boldsymbol{\epsilon}_{\theta}^{(2)}\left(\mathbf{x}_{\psi(\tau_{s1})}, \psi(\tau_{s1})\right) + O(h_{t}^{2}).$$
(A.13)

where  $\tau_{s1} - \tau_t = r_1 h_t$ . Combining (A.12) with Eq. (A.13), we have

$$\tilde{\mathbf{x}}_{s} = \frac{\alpha_{s}}{\alpha_{t}} \mathbf{x}_{t} + \alpha_{s} h_{t} \boldsymbol{\epsilon}_{\theta} \left( \mathbf{x}_{\psi(\tau_{s})}, \psi(\tau_{t}) \right) + \alpha_{s} \frac{h_{t}^{2}}{2} \frac{\boldsymbol{\epsilon}_{\theta} \left( \tilde{\mathbf{x}}_{\psi(\tau_{s})}, \psi(\tau_{s}) \right) - \boldsymbol{\epsilon}_{\theta} \left( \mathbf{x}_{\psi(\tau_{t})}, \psi(\tau_{t}) \right)}{\phi_{1}(m) r_{1} h_{t}} \\
- \alpha_{s} \frac{h_{t}^{2}}{2} \frac{\phi_{2}(m)}{\phi_{1}(m)} \boldsymbol{\epsilon}_{\theta}^{(1)} \left( \mathbf{x}_{\psi(\tau_{s})}, \psi(\tau_{s}) \right) + \alpha_{s} h_{t}^{3} \left( \frac{1}{6} - \frac{\phi_{3}(m) r_{1}}{2\phi_{1}(m)} \right) \boldsymbol{\epsilon}_{\theta}^{(2)} \left( \mathbf{x}_{\psi(\tau_{s})}, \psi(\tau_{s}) \right) \\
+ O(h_{t}^{4}). \tag{A.14}$$

By truncating the term containing  $h_t^2$  in Eq. (A.14), we obtain the algorithm shown in Algorithm 1:

$$\tilde{\mathbf{x}}_{s} \leftarrow \frac{\alpha_{s}}{\alpha_{t}} \mathbf{x}_{t} + \alpha_{s} h_{t} \boldsymbol{\epsilon}_{\theta} \left( \mathbf{x}_{\psi(\tau_{t})}, \psi(\tau_{t}) \right) + \alpha_{s} \frac{h_{t}}{2} \frac{\boldsymbol{\epsilon}_{\theta} \left( \tilde{\mathbf{x}}_{\psi(\tau_{s1})}, \psi(\tau_{s1}) \right) - \boldsymbol{\epsilon}_{\theta} \left( \mathbf{x}_{\psi(\tau_{t})}, \psi(\tau_{t}) \right)}{\phi_{1}(m) r_{1}}. \tag{A.15}$$

According to Eq. (A.14), it appears that we can easily conclude from Eq. (A.15) that the preliminary result has a local truncation error of  $O(h_t^2)$ . Nevertheless, our numerical experiments conducted on different datasets demonstrate that the algorithm 1 derived through this truncation method can generate high-quality samples with a restricted number of score function evaluations (NFE). Further details can be found in Appendix E. After careful observation, in fact, this technique partially eliminates the dependence on derivatives while still containing derivative-related information (such as the difference between two score function evaluations), thereby mitigating the error propagation caused by derivative estimation to a certain extent. By repeatedly using this technique, we can derive our SciRE-Solver-3 in Algorithm 2.

Note that if we have an even better estimate for  $\epsilon_{\theta}^{(1)}(\mathbf{x}_{\psi(\tau_{s1})}, \psi(\tau_{s1}))$ , we can further truncate the term containing  $h_t^3$ , leading to a generalized SciRE-Solver. We leave it for future study.

#### **A.4** Analytical Formulation of the function rNSR(·)

The computational costs associated with computing rNSR(·) are negligible. This is due to the fact that for the noise schedules of  $\alpha_t$  and  $\sigma_t$  employed in previous DPMs (referred to as "linear" and "cosine" in [2, 19]), both rNSR(·) and its inverse function NSR(t) have analytic formulations. We mainly consider the variance preserving type here, since it is the most widely-used type. The functions for other types (variance exploding and sub-variance preserving type) can be similarly derived.

Linear Noise Schedule [2]. In fact,

$$\log \alpha_t = -\frac{(\beta_1 - \beta_0)}{4} t^2 - \frac{\beta_0}{2} t,$$

where  $\beta_0 = 0.1$  and  $\beta_1 = 20$ , following [3, 13]. As  $\sigma_t = \sqrt{1 - \alpha_t^2}$ , we can compute NSR(t) analytically. Moreover, the inverse function is

$$t = \text{rNSR}(\tau) = \frac{1}{\beta_1 - \beta_0} \left( \sqrt{\beta_0^2 + 2(\beta_1 - \beta_0) \log(1 + \tau^2)} - \beta_0 \right),$$

where  $\tau = \text{NSR}(t)$ . To reduce the influence of numerical issues, we can compute t by the following equivalent formulation:

$$t = \text{rNSR}(\tau) = \frac{2\log(1+\tau^2)}{\sqrt{\beta_0^2 + 2(\beta_1 - \beta_0)\log(1+\tau^2) + \beta_0}}.$$

And we solve diffusion ODEs between  $[\epsilon, T]$ , where T = 1.

Cosine Noise Schedule [19]. Denote

$$\log \alpha_t = \log \left( \cos \left( \frac{\pi}{2} \cdot \frac{t+s}{1+s} \right) \right) - \log \left( \cos \left( \frac{\pi}{2} \cdot \frac{s}{1+s} \right) \right),$$

where s = 0.008, following [19]. As  $\sigma_t = \sqrt{1 - \alpha_t^2}$ , we can compute NSR(t) analytically. Denote  $\tau = \text{NSR}(t)$ , let

$$\varphi(\tau) = -\frac{1}{2}\log\left(1 + \tau^2\right)$$

which computes the corresponding  $\log \alpha$  for  $\tau$ . Then the inverse function is

$$t = \text{rNSR}(\tau) = \frac{2(1+s)}{\pi} \arccos\left(e^{\varphi(\tau) + \log\cos\left(\frac{\pi s}{2(1+s)}\right)}\right) - s.$$

And we solve diffusion ODEs between  $[\epsilon, T]$ , where T = 0.9946, following [13].

#### A.5 SciRE-Solver-agile

In order to facilitate the exploration of more possibilities of the SciRE-Solver our proposed and to fully utilize the given number of score function evaluations (NFE), we defined a simple combinatorial version based on SciRE-Solver-k and named as SciRE-Solver-agile. This version is based on whether the given NFE is divisible by k. If it is not divisible, solver-k is used as much as possible first, and then smaller order SciRE-Solver or DDIM are used to supplement.

To achieve this, when given a fixed budget N for the number of score function evaluations, we evenly divide the given interval into  $M = (\lfloor N/3 \rfloor + 1)$  segments. Subsequently, we carry out M sampling steps, adjusting based on the remainder R when dividing N by 3 to ensure a precise total of N evaluations.

When R=0, we initiate M-2 SciRE-Solver-3 steps, succeeded by 1 SciRE-Solver-2 step and 1 DDIM step. This results in a total of  $3 \cdot \left(\frac{N}{3}-1\right)+2+1=N$  evaluations. In the case of R=1, we begin with M-1 SciRE-Solver-3 steps, followed by 1 DDIM step. This

In the case of R = 1, we begin with M - 1 SciRE-Solver-3 steps, followed by 1 DDIM step. This yields a total of  $3 \cdot \left(\frac{N-1}{3}\right) + 1 = N$  evaluations.

Lastly, when R = 2, we conduct M - 1 SciRE-Solver-3 steps, succeeded by 1 SciRE-Solver-2 step. This leads to a cumulative count of  $3 \cdot \left(\frac{N-2}{3}\right) + 2 = N$  score function evaluations.

Our empirical observations show that using this time step design can enhance the quality of image generation. With the implementation of the SciRE-Solver algorithm, high-quality samples can be generated in just 20 steps, such as achieving a 2.42 FID result on CIFAR-10 with just 20 NFE.

#### A.6 Sampling from Discrete-Time DPMs

SciRE-Solver aims to solve continuous-time diffusion ODEs. For DPMs trained on discrete-time labels, we need to firstly wrap the model function to a noise prediction model that accepts the continuous time as the input. In the subsequent discussion, we examine the broader scenario of discrete-time DPMs, specifically focusing on two variants: the 1000-step DPMs [2] and the 4000-step

DPMs [19]. Discrete-time DPMs [2] train the noise prediction model at N fixed time steps  $\{t_n\}_{n=1}^N$ , and the value of N is typically set to either 1000 or 4000 in practice. The implementation of the 4000-step DPMs [19] entails mapping the time steps of the 4000-step DPMs to the range of the 1000-step DPMs. Specifically, the noise prediction model is parameterized as  $\tilde{\epsilon}_{\theta}(\mathbf{x}_n, \frac{1000n}{N})$ , where  $\mathbf{x}_n$ is corresponding to the value at time  $t_{n+1}$ , and n ranges from 0 to N-1. In practice, these discrete-time

DPMs commonly employ uniform time steps between [0, T], then  $t_n = \frac{nT}{N}$ , for n = 1, ..., N. As sated by Lu et al. [13], the discrete-time noise prediction model is limited in predicting noise levels for times less than the smallest time  $t_1$ . Given that  $t_1 = \frac{T}{N}$  and the corresponding discrete-time noise prediction model at time  $t_1$  is  $\tilde{\epsilon}_{\theta}(\mathbf{x}_0, 0)$ , it is necessary to "scale" the discrete time steps from  $[t_1, t_N] = \left[\frac{T}{N}, T\right]$  to the continuous time range  $[\epsilon, T]$ . However, the question of which scaling approach would be beneficial to the corresponding sampling algorithm remains an open problem. In our codebase, we employ two types of scaling recommended by Lu et al. [13] as follows.

**Discrete-1.** Let  $\epsilon_{\theta}(\cdot, t) = \epsilon_{\theta}(\cdot, \frac{T}{N})$  for  $t \in [\epsilon, \frac{T}{N}]$ , and scale the discrete time steps  $[t_1, t_N] = [\frac{T}{N}, T]$  to the continuous time range  $\left[\frac{T}{N}, T\right]$ . In this case, the continuous-time noise prediction model is defined by

$$\epsilon_{\theta}(\mathbf{x}, t) = \tilde{\epsilon}_{\theta}\left(\mathbf{x}, 1000 \cdot \max\left(t - \frac{T}{N}, 0\right)\right),$$

where the continuous time  $t \in \left[\epsilon, \frac{T}{N}\right]$  maps to the discrete input 0, and the continuous time T maps to the discrete input  $\frac{1000(N-1)}{N}$ 

**Discrete-2.** Scale the discrete time steps  $[t_1, t_N] = \left[\frac{T}{N}, T\right]$  to the continuous time range [0, T]. In this case, the continuous-time noise prediction model is defined by

$$\epsilon_{\theta}(\mathbf{x}, t) = \tilde{\epsilon}_{\theta} \left( \mathbf{x}, 1000 \cdot \frac{(N-1)t}{NT} \right),$$

where the continuous time 0 maps to the discrete input 0, and the continuous time T maps to the discrete input  $\frac{1000(N-1)}{N}$ . By such reparameterization, the noise prediction model can adopt the continuous-time steps as input,

which enables SciRE-Solver to perform sampling not only for continuous-time DPMs but also for discrete-time DPMs.

#### A.7 Conditional Sampling by SciRE-Solver

With a simple modification, following the settings provided by Lu et al. [13], SciRE-Solver can be used for conditional sampling. The conditional generation requires sampling from a conditional diffusion ODE, as stated in [3, 4]. Specifically, by following the classifier guidance method [4], the conditional noise prediction model can defined as  $\epsilon_{\theta}(\mathbf{x}_t, t, y) := \epsilon_{\theta}(\mathbf{x}_t, t) - s \cdot \sigma_t \nabla_{\mathbf{x}} \log p_t(y \mid \mathbf{x}_t; \theta)$ . Here,  $p_t(y | \mathbf{x}_t; \theta)$  represents a pre-trained classifier, and s denotes the classifier guidance scale. Thus, one can utilize SciRE-Solver to solve this diffusion ODE for fast conditional sampling.

## A.8 Supported Models

SciRE-solver support four types of diffusion probabilistic models, including the noise prediction model  $\epsilon_{\theta}$  [2, 34], the data prediction model  $\mathbf{x}_{\theta}$  [6], the velocity prediction model  $\mathbf{v}_{\theta}$  [7] and marginal score function  $s_{\theta}[3]$ . Here, we follow the configurations provided by Lu et al. in [13, 35].

## Appendix B Proof of Proposition 3.1

Consider the following stochastic differential equation (SDE):

$$d\mathbf{x}_{t} = f(t)\mathbf{x}_{t} dt + g(t)d\omega_{t}, \quad \mathbf{x}_{0} \sim q_{0}(\mathbf{x}_{0}),$$
(B.1)

where  $\omega_t \in \mathbb{R}^D$  is the standard Wiener process, and

$$f(t) = \frac{d \log \alpha_t}{dt}, \quad g^2(t) = \frac{d\sigma_t^2}{dt} - 2\frac{d \log \alpha_t}{dt}\sigma_t^2.$$
 (B.2)

Here  $\alpha_t, \sigma_t \in \mathbb{R}^+$  are differentiable function of time t with bounded derivatives. The choice for  $\alpha_t$  and  $\sigma_t$  is known as the *noise schedule* of a DPM.

Song et al. [3] defined the following diffusion ODE for Eq. (B.1):

$$\frac{\mathrm{d}\mathbf{x}_{t}}{\mathrm{d}t} = f(t)\mathbf{x}_{t} + \frac{g^{2}(t)}{2\sigma_{t}}\boldsymbol{\epsilon}_{\theta}\left(\mathbf{x}_{t}, t\right), \quad \mathbf{x}_{T} \sim \mathcal{N}\left(\mathbf{0}, \hat{\sigma}^{2} \boldsymbol{I}\right), \tag{B.3}$$

where  $\epsilon_{\theta}(\mathbf{x}_t, t)$  is the trained scale score function. The exact solution of the above semi-linear ODE can be formulated by the *variation-of-constants* formula [31]:

$$\mathbf{x}_{t} = e^{\int_{s}^{t} f(\lambda) d\lambda} \left( \int_{s}^{t} h(\lambda) \boldsymbol{\epsilon}_{\theta} \left( \mathbf{x}_{\lambda}, \lambda \right) d\lambda + \mathbf{x}_{s} \right), \tag{B.4}$$

where  $h(\lambda) := e^{-\int_s^{\lambda} f(z)dz} \frac{g^2(\lambda)}{2\sigma_{\lambda}}$ , and  $\mathbf{x}_s$  represents the given initial value. Since  $f(\lambda) = \frac{d \log(\alpha_{\lambda})}{d\lambda}$ , thus  $h(\lambda) = \frac{\alpha_s}{\alpha_{\lambda}} \frac{g^2(\lambda)}{2\sigma_{\lambda}}$ . We observe that  $h(\lambda)$  can be rewritten as

$$h(\lambda) = \frac{\alpha_s}{2\alpha_\lambda \sigma_\lambda} \left( \frac{d\sigma_\lambda^2}{d\lambda} - 2 \frac{d\log \alpha_\lambda}{d\lambda} \sigma_\lambda^2 \right) = \frac{\alpha_s}{\alpha_\lambda} \left( \frac{d\sigma_\lambda}{d\lambda} - \frac{\sigma_\lambda}{\alpha_\lambda} \frac{d\alpha_\lambda}{d\lambda} \right) = \alpha_s \frac{dNSR(\lambda)}{d\lambda}, \tag{B.5}$$

where  $NSR(\lambda) := \frac{\sigma_{\lambda}}{\alpha_{\lambda}}$ , and we refer to it as the time-dependent *signal-to-noise-ratio* function. Note that the signal-to-noise-ratio function defined above differs from the definition presented in [29] by a squared relationship between the two. Then, we can rewrite Eq. (B.4) as

$$\mathbf{x}_{t} = \frac{\alpha_{t}}{\alpha_{s}} \mathbf{x}_{s} + \alpha_{t} \int_{s}^{t} \frac{d\text{NSR}(\lambda)}{d\lambda} \boldsymbol{\epsilon}_{\theta} \left( \mathbf{x}_{\lambda}, \lambda \right) d\lambda. \tag{B.6}$$

Since NSR(·) is a monotonically function w.r.t. time, it has a reverse function rNSR(·) satisfying t = rNSR(NSR(t)). Thus, using the *change-of-variable* for NSR( $\lambda$ ) to Eq. (B.6), we can obtain

$$\mathbf{x}_{t} = \frac{\alpha_{t}}{\alpha_{s}} \mathbf{x}_{s} + \alpha_{t} \int_{s}^{t} \frac{d\mathrm{NSR}(\lambda)}{d\lambda} \boldsymbol{\epsilon}_{\theta} (\mathbf{x}_{\lambda}, \lambda) d\lambda$$

$$= \frac{\alpha_{t}}{\alpha_{s}} \mathbf{x}_{s} + \alpha_{t} \int_{s}^{t} \boldsymbol{\epsilon}_{\theta} (\mathbf{x}_{\lambda}, \lambda) d\mathrm{NSR}(\lambda)$$

$$= \frac{\alpha_{t}}{\alpha_{s}} \mathbf{x}_{s} + \alpha_{t} \int_{\mathrm{NSR}(s)}^{\mathrm{NSR}(t)} \boldsymbol{\epsilon}_{\theta} (\mathbf{x}_{\mathrm{rNSR}(\tau)}, \mathrm{rNSR}(\tau)) d\tau.$$
(B.7)

Now we complete the proof the Proposition 3.1.

**Hints** We observe that the integral term on the r.h.s. of Eq. (B.7) appears to be a traditional integration problem, and we could use conventional numerical methods for solving integrals to evaluate it. However, caution must be taken when using such methods, given that the integrand is only an approximation of the scaled score function and its explicit expression is unknown. Therefore, traditional techniques may magnify the numerical error in these scenarios. Nonetheless, the DPM-Solver provides an inspiring example of how traditional algorithmic concepts can be combined with practical considerations to create numerical algorithms that are appropriate for diffusion ODEs.

## **Appendix C** Proof of Theorem 3.1 and Corollary 1

## C.1 Preliminaries

Throughout this section, we denote  $NSR_{min} := \min_{i} \{NSR(t_i)\}, NSR_{max} := \max_{i} \{NSR(t_i)\}, \text{ and assume } \{NSR(t_i)\}$ 

that  $\epsilon_{\theta}\left(\mathbf{x}_{\psi(\tau)},\psi(\tau)\right) \in \mathbb{C}^{\infty}[\mathrm{NSR}_{\min},\mathrm{NSR}_{\max}]$ , which means that the total derivatives  $\frac{\mathrm{d}^{k}\epsilon_{\theta}(\mathbf{x}_{\psi(\tau)},\psi(\tau))}{\mathrm{d}\tau^{k}}$  exist and are continuous for  $k \in \mathbb{Z}_{+}$ . Notice that  $\tau := \mathrm{NSR}(t), \psi(\tau) := \mathrm{rNSR}(\tau)$  and the reverse function of NSR, i.e. rNSR, satisfying  $t = \mathrm{rNSR}(\mathrm{NSR}(t)) = \psi(\tau)$ . Denote  $h_{s} := \mathrm{NSR}(t) - \mathrm{NSR}(s) = \tau_{t} - \tau_{s}$ , and  $\epsilon_{\theta}^{(k)}\left(\mathbf{x}_{\psi(\tau)},\psi(\tau)\right) := \frac{\mathrm{d}^{k}\epsilon_{\theta}\left(\mathbf{x}_{\psi(\tau)},\psi(\tau)\right)}{\mathrm{d}\tau^{k}}$  as k-th order total derivative of  $\epsilon_{\theta}\left(\mathbf{x}_{\psi(\tau)},\psi(\tau)\right)$  w.r.t.  $\tau$ . For  $n \geq 1$ , the n-th order Taylor expansion of  $\epsilon_{\theta}\left(\mathbf{x}_{\psi(\tau)},\psi(\tau_{t})\right)$  w.r.t.  $\tau$  at  $\tau_{s}$  is

$$\boldsymbol{\epsilon}_{\theta} \left( \mathbf{x}_{\psi(\tau_t)}, \psi(\tau_t) \right) = \sum_{k=0}^{n} \frac{h_s^k}{k!} \boldsymbol{\epsilon}_{\theta}^{(k)} \left( \mathbf{x}_{\psi(\tau_s)}, \psi(\tau_s) \right) + O(h_s^{n+1}). \tag{C.1}$$

For any  $k \ge 0$ , we can approximate the k-th order total derivative term  $\epsilon_{\theta}^{(k)}\left(\mathbf{x}_{\psi(\tau_s)}, \psi(\tau_s)\right)$  in Eq. (C.1) by using the first-order difference formula:

$$\boldsymbol{\epsilon}_{\theta}^{(k)}\left(\mathbf{x}_{\psi(\tau_s)}, \psi(\tau_s)\right) = \frac{\boldsymbol{\epsilon}_{\theta}^{(k-1)}\left(\mathbf{x}_{\psi(\tau_t)}, \psi(\tau_t)\right) - \boldsymbol{\epsilon}_{\theta}^{(k-1)}\left(\mathbf{x}_{\psi(\tau_s)}, \psi(\tau_s)\right)}{h_s} - O(h_s). \tag{C.2}$$

For ease of notation, we denote  $\epsilon_{\theta}^{(k)}\left(\mathbf{x}_{\psi(\tau)},\psi(\tau)\right)$  as  $\Gamma^{(k)}(\tau)$ . Notice that  $\epsilon_{\theta}\left(\mathbf{x}_{\psi(\tau)},\psi(\tau)\right) = \Gamma^{(0)}(\tau)$ . Then Eq. (C.2) can be represented as:

$$\Gamma^{(k)}(\tau_s) = \frac{\Gamma^{(k-1)}(\tau_t) - \Gamma^{(k-1)}(\tau_s)}{h_s} - O(h_s). \tag{C.3}$$

#### C.2 Proof of Theorem 3.1

*Proof.* While  $n \to \infty$ , Eq. (C.1) becomes:

$$\Gamma^{(0)}(\tau_t) = \sum_{k=0}^{\infty} \frac{h_s^k}{k!} \Gamma^{(k)}(\tau_s)$$

$$= \Gamma^{(0)}(\tau_s) + \sum_{k=1}^{\infty} \frac{h_s^k}{k!} \Gamma^{(k)}(\tau_s).$$
(C.4)

Moving  $\Gamma^{(0)}(\tau_s)$  from the right-hand side of the above equation to the left-hand side and then dividing both sides of the equation by  $h_s$ , we can obtain:

$$\begin{split} &\frac{\Gamma^{(0)}(\tau_{I}) - \Gamma^{(0)}(\tau_{s})}{h_{s}} \\ &= \sum_{k=1}^{\infty} \frac{h_{s}^{k-1}}{k!} \Gamma^{(k)}(\tau_{s}) \\ &= \Gamma^{(1)}(\tau_{s}) + \sum_{k=2}^{\infty} \frac{h_{s}^{k-1}}{k!} \Gamma^{(k)}(\tau_{s}) \\ &= \Gamma^{(1)}(\tau_{s}) + \sum_{k=2}^{\infty} \frac{h_{s}^{k-1}}{k!} \left( \frac{\Gamma^{(k-1)}(\tau_{I}) - \Gamma^{(k-1)}(\tau_{s})}{h_{s}} - O(h_{s}) \right) \\ &= \Gamma^{(1)}(\tau_{s}) + \sum_{k=2}^{\infty} \frac{h_{s}^{k-2}}{k!} \left( \Gamma^{(k-1)}(\tau_{I}) - \Gamma^{(k-1)}(\tau_{s}) \right) - \sum_{k=2}^{\infty} \frac{h_{s}^{k-1}}{k!} O(h_{s}) \\ &= \Gamma^{(1)}(\tau_{s}) + \sum_{k=2}^{\infty} \frac{h_{s}^{k-2}}{k!} \Gamma^{(k-1)}(\tau_{s}) + \sum_{k=2}^{\infty} \frac{h_{s}^{k-2}}{k!} \Gamma^{(k-1)}(\tau_{I}) - Q \\ &= \left( 1 - \frac{1}{2} \right) \Gamma^{(1)}(\tau_{s}) - \sum_{k=3}^{\infty} \frac{h_{s}^{k-2}}{k!} \Gamma^{(k-1)}(\tau_{s}) + R_{1} - Q \\ &= \left( 1 - \frac{1}{2} \right) \Gamma^{(1)}(\tau_{s}) + \sum_{k=3}^{\infty} \frac{h_{s}^{k-3}}{k!} \Gamma^{(k-2)}(\tau_{I}) - \Gamma^{(k-2)}(\tau_{s}) - O(h_{s}^{2}) \right) + R_{1} - Q \\ &= \left( 1 - \frac{1}{2} \right) \Gamma^{(1)}(\tau_{s}) + \sum_{k=3}^{\infty} \frac{h_{s}^{k-3}}{k!} \Gamma^{(k-2)}(\tau_{s}) - \sum_{k=3}^{\infty} \frac{h_{s}^{k-3}}{k!} \Gamma^{(k-2)}(\tau_{I}) - O(h_{s}^{2}) + R_{1} \\ &= \left( 1 - \frac{1}{2} + \frac{1}{6} \right) \Gamma^{(1)}(\tau_{s}) + \sum_{k=4}^{\infty} \frac{h_{s}^{k-3}}{k!} \Gamma^{(k-2)}(\tau_{s}) + R_{2} + R_{1} - O(h_{s}^{2}) \\ &= \left( 1 - \frac{1}{2} + \frac{1}{3!} - \frac{1}{4!} \right) \Gamma^{(1)}(\tau_{s}) + \sum_{k=4}^{\infty} \frac{h_{s}^{k-3}}{k!} \Gamma^{(k-3)}(\tau_{s}) + R_{1} + R_{2} + R_{3} - O(h_{s}^{2}) \\ &\cdots \\ &= \sum_{k=1}^{\infty} \frac{(-1)^{k-1}}{k!} \Gamma^{(1)}(\tau_{s}) + \sum_{k=1}^{\infty} R_{l} - O(h_{s}^{2}), \end{split}$$

where

$$R_{1} = \sum_{k=2}^{\infty} \frac{h_{s}^{k-2}}{k!} \Gamma^{(k-1)}(\tau_{t})$$

$$R_{2} = -\sum_{k=3}^{\infty} \frac{h_{s}^{k-3}}{k!} \Gamma^{(k-2)}(\tau_{t})$$

$$R_{3} = \sum_{k=4}^{\infty} \frac{h_{s}^{k-4}}{k!} \Gamma^{(k-3)}(\tau_{t})$$
...
(C.6)

 $R_i = (-1)^{i+1} \sum_{k=i+1}^{\infty} \frac{h_s^{k-i-1}}{k!} \Gamma^{(k-i)}(\tau_t), \quad i \in \mathbb{Z}_+.$ 

Adding the first term and second term of  $R_i$ ,  $i \in \mathbb{Z}_+$  separately, we can derive

$$\sum_{i=1}^{\infty} R_i = \sum_{k=2}^{\infty} \frac{(-1)^k}{k!} \Gamma^{(1)}(\tau_t) + \sum_{k=3}^{\infty} \frac{(-1)^{k+1} h_s}{k!} \Gamma^{(2)}(\tau_t) + \underbrace{\sum_{i=3}^{\infty} \sum_{k=i+1}^{\infty} \frac{(-1)^{k+i-1} h_s^{i-1}}{k!} \Gamma^{(i)}(\tau_t)}_{O(h^2)}.$$
(C.7)

Notice that

$$\sum_{i=3}^{\infty} \sum_{k=i+1}^{\infty} \frac{(-1)^{k+i-1} h_s^{i-1}}{k!} \Gamma^{(i)}(\tau_t) = \sum_{i=3}^{\infty} (-1)^{i-1} h_s^{i-1} \Gamma^{(i)}(\tau_t) \sum_{k=i+1}^{\infty} \frac{(-1)^k}{k!} = O(h_s^2), \tag{C.8}$$

because  $\sum_{k=i+1}^{\infty} \frac{(-1)^k}{k!}$ ,  $\forall i \in \mathbb{Z}_+$  are all convergent alternating series which can be easily proved with Leibniz's test. Then Eq. (C.5) can be shown as:

$$\frac{\Gamma^{(0)}(\tau_t) - \Gamma^{(0)}(\tau_s)}{h_s} = \sum_{k=1}^{\infty} \frac{(-1)^{k-1}}{k!} \Gamma^{(1)}(\tau_s) + \sum_{i=1}^{2} \sum_{k=i+1}^{\infty} \frac{(-1)^{k+i-1} h_s^{i-1}}{k!} \Gamma^{(i)}(\tau_t) - O(h_s^2). \tag{C.9}$$

Consequently, we can get  $\Gamma^{(1)}(\tau_s)$  by simple manipulation of rearranging and affine transformation applied to above equation:

$$\Gamma^{(1)}(\tau_s) = \frac{e}{e-1} \frac{\Gamma^{(0)}(\tau_t) - \Gamma^{(0)}(\tau_s)}{h_s} - \frac{e}{e-1} \sum_{i=1}^{2} \sum_{k=i+1}^{\infty} \frac{(-1)^{k+i-1} h_s^{i-1}}{k!} \Gamma^{(i)}(\tau_t) + O(h_s^2) 
= \frac{e}{e-1} \frac{\Gamma^{(0)}(\tau_t) - \Gamma^{(0)}(\tau_s)}{h_s} - \frac{e}{e-1} \left( \frac{1}{e} \Gamma^{(1)}(\tau_t) + \frac{e-2}{2e} h_s \Gamma^{(2)}(\tau_t) \right) + O(h_s^2) 
= \frac{e}{e-1} \frac{\Gamma^{(0)}(\tau_t) - \Gamma^{(0)}(\tau_s)}{h_s} - \frac{\Gamma^{(1)}(\tau_t)}{e-1} - \frac{(e-2)h_s}{2(e-1)} \Gamma^{(2)}(\tau_t) + O(h_s^2),$$
(C.10)

where

$$\sum_{k=1}^{\infty} \frac{(-1)^{k-1}}{k!} = 1 - e^{-1}$$

$$\sum_{k=2}^{\infty} \frac{(-1)^k}{k!} = e^{-1}$$

$$\sum_{k=3}^{\infty} \frac{(-1)^{k+1}}{k!} = -e^{-1} + \frac{1}{2} = \frac{e-2}{2e},$$
(C.11)

for  $e^x = \sum_{k=0}^{\infty} \frac{x^k}{k!}$  with x = -1.

Notice that we denote  $\boldsymbol{\epsilon}_{\theta}^{(k)}\left(\mathbf{x}_{\psi(\tau)},\psi(\tau)\right)$  as  $\Gamma^{(k)}(\tau)$ . While using  $\tilde{\mathbf{x}}$  to approximate  $\mathbf{x}$  and replacing the terms like  $\Gamma^{(k)}(\tau)$  in Eq. (C.10) with terms like  $\boldsymbol{\epsilon}_{\theta}^{(k)}\left(\mathbf{x}_{\psi(\tau)},\psi(\tau)\right)$ , we can get the results shown in Theorem 3.1.

#### C.3 Proof of Corollary 1

We observe that the differentiability constraint imposed by Theorem 3.1 appears to be rather restrictive. In order to enhance its broad applicability, we further propose a recursive derivative estimation method under the assumption of limited differentiability. The corresponding proof process is as follows: Proof Assume that  $F_0(\mathbf{x}_{(1)}, \mu(\tau)) \in \mathbb{C}^n[NSR_{min}]$  While n is a finite positive integer. Fig.

*Proof.* Assume that  $\epsilon_{\theta}(\mathbf{x}_{\psi(\tau)}, \psi(\tau)) \in \mathbb{C}^n[\mathrm{NSR}_{\min}, \mathrm{NSR}_{\max}]$ . While n is a finite positive integer, Eq. (C.1) becomes:

$$\Gamma^{(0)}(\tau_t) = \sum_{k=0}^{n} \frac{h_s^k}{k!} \Gamma^{(k)}(\tau_s) + O(h_s^{n+1})$$

$$= \Gamma^{(0)}(\tau_s) + \sum_{k=1}^{n} \frac{h_s^k}{k!} \Gamma^{(k)}(\tau_s) + O(h_s^{n+1}).$$
(C.12)

Same as the derivation process in (C.5), we can obtain

$$\frac{\Gamma^{(0)}(\tau_{t}) - \Gamma^{(0)}(\tau_{s})}{h_{s}} = \sum_{k=1}^{n} \frac{h_{s}^{k-1}}{k!} \Gamma^{(k)}(\tau_{s}) + O(h_{s}^{n}) 
= \Gamma^{(1)}(\tau_{s}) + \sum_{k=2}^{n} \frac{h_{s}^{k-1}}{k!} \Gamma^{(k)}(\tau_{s}) + O(h_{s}^{n}) 
= \Gamma^{(1)}(\tau_{s}) - \sum_{k=2}^{n} \frac{h_{s}^{k-2}}{k!} \Gamma^{(k-1)}(\tau_{s}) + \sum_{k=2}^{n} \frac{h_{s}^{k-2}}{k!} \Gamma^{(k-1)}(\tau_{t}) - O(h_{s}^{2}) + O(h_{s}^{n}) 
O(h_{s}^{2}) - O(h_{s}^{2}) + O(h_{s}^{n}) 
= \left(1 - \frac{1}{2}\right) \Gamma^{(1)}(\tau_{s}) + \sum_{k=3}^{n} \frac{h_{s}^{k-3}}{k!} \Gamma^{(k-2)}(\tau_{s}) - \sum_{k=3}^{n} \frac{h_{s}^{k-3}}{k!} \Gamma^{(k-2)}(\tau_{t}) - O(h_{s}^{2}) + R_{1}$$

$$= \left(1 - \frac{1}{2} + \frac{1}{6}\right) \Gamma^{(1)}(\tau_{s}) - \sum_{k=4}^{n} \frac{h_{s}^{k-4}}{k!} \Gamma^{(k-3)}(\tau_{s}) + \sum_{k=4}^{n} \frac{h_{s}^{k-4}}{k!} \Gamma^{(k-3)}(\tau_{t}) - O(h_{s}^{2}) + R_{1} + R_{2}$$

$$\dots$$

$$= \sum_{k=1}^{n} \frac{(-1)^{k-1}}{k!} \Gamma^{(1)}(\tau_{s}) + \sum_{i=1}^{n-1} R_{i} - O(h_{s}^{2}),$$

where

$$R_{1} = \sum_{k=2}^{n} \frac{h_{s}^{k-2}}{k!} \Gamma^{(k-1)}(\tau_{t})$$

$$R_{2} = -\sum_{k=3}^{n} \frac{h_{s}^{k-3}}{k!} \Gamma^{(k-2)}(\tau_{t})$$

$$R_{3} = \sum_{k=4}^{n} \frac{h_{s}^{k-4}}{k!} \Gamma^{(k-3)}(\tau_{t})$$

$$\dots$$

$$R_{n-1} = (-1)^{n} \sum_{t=1}^{n} \frac{h_{s}^{k-n}}{k!} \Gamma^{(k-n+1)}(\tau_{t}).$$
(C.14)

Hence adding the first term and second term of  $R_i$ , i = 1, 2, ..., n-1 separately, we also have

$$\sum_{i=1}^{n-1} R_i = \sum_{k=2}^{n} \frac{(-1)^k}{k!} \Gamma^{(1)}(\tau_t) + \sum_{k=3}^{n} \frac{(-1)^{k+1} h_s}{k!} \Gamma^{(2)}(\tau_t) + \sum_{i=3}^{n-1} \sum_{k=i+1}^{n} \frac{(-1)^{k+i-1} h_s^{i-1}}{k!} \Gamma^{(i)}(\tau_t) 
= \sum_{k=2}^{n} \frac{(-1)^k}{k!} \Gamma^{(1)}(\tau_t) + \sum_{k=3}^{n} \frac{(-1)^{k+1} h_s}{k!} \Gamma^{(2)}(\tau_t) + O(h_s^2).$$
(C.15)

Denote  $\phi_1(n) = \sum_{k=1}^n \frac{(-1)^{k-1}}{k!}$ ,  $\phi_2(n) = \sum_{k=2}^n \frac{(-1)^k}{k!}$ , and  $\phi_3(n) = \sum_{k=3}^n \frac{(-1)^{k+1}}{k!}$ . Combining (C.13) and (C.15), we can easily derive  $\Gamma(\tau_s, 1)$  by

$$\Gamma^{(1)}(\tau_s) = \frac{1}{\phi_1(n)} \frac{\Gamma^{(0)}(\tau_t) - \Gamma^{(0)}(\tau_s)}{h_s} - \frac{\phi_2(n)}{\phi_1(n)} \Gamma^{(1)}(\tau_t) - \frac{\phi_3(n)h_s}{\phi_1(n)} \Gamma^{(2)}(\tau_t) + O(h_s^2). \tag{C.16}$$

Similarly, while using  $\tilde{\mathbf{x}}$  to approximate  $\mathbf{x}$  and replacing the terms like  $\Gamma^{(k)}(\tau)$  in Eq. (C.16) with terms like  $\epsilon_{\theta}^{(k)}(\mathbf{x}_{\psi(\tau)}, \psi(\tau))$ , we can get the results shown in Corollary 1.

## Appendix D Proof of Theorem 3.2

Moreover, under reasonable assumptions, SciRE-Solver-k is a k-th order solver.

#### **D.1** Preliminaries

**Assumption D.1** The function  $\epsilon_{\theta}(\mathbf{x}_t, t)$  is set to be in  $\mathbb{C}^m$ , meaning that  $\epsilon_{\theta}(\mathbf{x}_t, t)$  is m times continuously differentiable. Specifically,  $m \geq 3$  in this paper.

**Assumption D.2**  $\epsilon_{\theta}(\mathbf{x}_{t},t)$  is a Lipschitz continuous function w.r.t.  $\mathbf{x}_{t}$ .

**Assumption D.3** For  $\forall t$ , there exists  $\delta > 0$  such that  $\exists \rho \in \mathbb{U}(t,\delta), (l+\frac{1}{2^n})\boldsymbol{\epsilon}_{\theta}^{(1)}(\mathbf{x}_t,t) = l(1+\frac{1}{2^n})\boldsymbol{\epsilon}_{\theta}^{(1)}(\mathbf{x}_t,t) = l\boldsymbol{\epsilon}_{\theta}^{(1)}(\mathbf{x}_t,t) = l\boldsymbol{\epsilon}_{\theta}^{$ 

As in Appendix C, we denote  $\tau := \text{NSR}(t)$ ,  $\psi(\tau) := \text{rNSR}(\tau)$  and  $h_s := \tau_t - \tau_s$ . In Appendix B, we transform the form of the solution to diffusion ODEs as in Eq. (B.6) to the form as in (B.7) by using the change of variable formula. The resulting solution can be formed as:

$$\mathbf{x}_{t} = \frac{\alpha_{t}}{\alpha_{s}} \mathbf{x}_{s} + \alpha_{t} \int_{\tau_{s}}^{\tau_{t}} \boldsymbol{\epsilon}_{\theta} \left( \mathbf{x}_{\psi(\tau)}, \psi(\tau) \right) d\tau. \tag{D.1}$$

Then by substituting the *n*-th order Taylor expansion of  $\epsilon_{\theta} \left( \mathbf{x}_{\psi(\tau_t)}, \psi(\tau_t) \right)$  w.r.t.  $\tau$  at  $\tau_s$ 

$$\boldsymbol{\epsilon}_{\theta} \left( \mathbf{x}_{\psi(\tau_{t})}, \psi(\tau_{t}) \right) = \sum_{k=0}^{n} \frac{h_{s}^{k}}{k!} \boldsymbol{\epsilon}_{\theta}^{(k)} \left( \mathbf{x}_{\psi(\tau_{s})}, \psi(\tau_{s}) \right) + O(h_{s}^{n+1}), \tag{D.2}$$

for the  $\epsilon_{\theta}(\mathbf{x}_{\psi(\tau_t)}, \psi(\tau_t))$  in Eq. (D.1), we can derive the exact solution of  $\mathbf{x}_t$  in Eq. (D.1) as follows:

$$\mathbf{x}_{t} = \frac{\alpha_{t}}{\alpha_{s}} \mathbf{x}_{s} + \alpha_{t} \sum_{k=0}^{n} \frac{h_{s}^{k+1}}{(k+1)!} \boldsymbol{\epsilon}_{\theta}^{(k)} \left( \mathbf{x}_{\psi(\tau_{s})}, \psi(\tau_{s}) \right) + O(h_{s}^{n+2})$$

$$= \frac{\alpha_{t}}{\alpha_{s}} \mathbf{x}_{s} + \alpha_{t} \sum_{k=0}^{n} \frac{h_{s}^{k+1}}{(k+1)!} \boldsymbol{\epsilon}_{\theta}^{(k)} \left( \mathbf{x}_{s}, s \right) + O(h_{s}^{n+2}). \tag{D.3}$$

## **D.2** Proof of Theorem 3.2 when k = 2

In this subsection, we prove the global convergence order of SciRE-Solver-2 is no less than 1 and is 2 under reasonable assumptions.

*Proof.* For each iteration step, we first update according to:

$$h_s = \tau_t - \tau_s,\tag{D.4}$$

$$s_1 = \psi(\tau_s + r_1 h_s),\tag{D.5}$$

$$\mathbf{u}_1 = \frac{\alpha_{s_1}}{\alpha_s} \mathbf{x}_s + \alpha_{s_1} r_1 h_s \boldsymbol{\epsilon}_{\theta} \left( \mathbf{x}_s, s \right), \tag{D.6}$$

$$\tilde{\mathbf{x}}_{t} = \frac{\alpha_{t}}{\alpha_{s}} \mathbf{x}_{s} + \alpha_{t} h_{s} \boldsymbol{\epsilon}_{\theta} \left( \mathbf{x}_{s}, s \right) + \alpha_{t} \frac{h_{s}^{2}}{2\phi_{1}(m) r_{1} h_{s}} \left( \boldsymbol{\epsilon}_{\theta} \left( \mathbf{u}_{1}, s_{1} \right) - \boldsymbol{\epsilon}_{\theta} \left( \mathbf{x}_{s}, s \right) \right), \tag{D.7}$$

where  $\tilde{\mathbf{x}}_t$  denotes the approximate solution of  $\mathbf{x}_t$  computed by SciRE-Solver-2,  $r_1 \in (0, 1)$  is a hyperparameter so that  $s_1 \in (t, s)$ .

Next, taking n = 1 in Eq. (D.3), we can get the exact solution of  $\mathbf{x}_t$  as follows:

$$\mathbf{x}_{t} = \frac{\alpha_{t}}{\alpha_{s}} \mathbf{x}_{s} + \alpha_{t} h_{s} \boldsymbol{\epsilon}_{\theta} \left( \mathbf{x}_{s}, s \right) + \alpha_{t} \frac{h_{s}^{2}}{2} \boldsymbol{\epsilon}_{\theta}^{(1)} \left( \mathbf{x}_{s}, s \right) + O(h_{s}^{3})$$
(D.8)

Then by subtracting the last equation from Eq. (D.7) and using  $\mathbf{u}_1 - \mathbf{x}_{s_1} = O(h_s^2)$ , we have

$$\frac{\mathbf{x}_{t} - \tilde{\mathbf{x}}_{t}}{\alpha_{t}} = \frac{h_{s}^{2}}{2} \boldsymbol{\epsilon}_{\theta}^{(1)}(\mathbf{x}_{s}, s) - \frac{h_{s}^{2}}{2\phi_{1}(m)r_{1}h_{s}} (\boldsymbol{\epsilon}_{\theta}(\mathbf{u}_{1}, s_{1}) - \boldsymbol{\epsilon}_{\theta}(\mathbf{x}_{s}, s)) + O(h_{s}^{4})$$

$$= \frac{h_{s}^{2}}{2} \left( \boldsymbol{\epsilon}_{\theta}^{(1)}(\mathbf{x}_{s}, s) - \frac{\boldsymbol{\epsilon}_{\theta}(\mathbf{x}_{s_{1}}, s_{1}) - \boldsymbol{\epsilon}_{\theta}(\mathbf{x}_{s}, s)}{\phi_{1}(m)r_{1}h_{s}} \right) + O(h_{s}^{3}), \tag{D.9}$$

where  $\|\boldsymbol{\epsilon}_{\theta}(\mathbf{u}_1, s_1) - \boldsymbol{\epsilon}_{\theta}(\mathbf{x}_{s_1}, s_1)\| = O(\|\mathbf{u}_1 - \mathbf{x}_{s_1}\|) = O(h_s^2)$  under Assumption D.2. By Assumption D.2 and Lagrange's mean value theorem, we find that

$$\|\boldsymbol{\epsilon}_{\theta}(\mathbf{x}_{s_{1}}, s_{1}) - \boldsymbol{\epsilon}_{\theta}(\mathbf{x}_{s}, s)\| \le L\|\mathbf{x}_{s_{1}} - \mathbf{x}_{s}\| = L\|\mathbf{x}_{n}'(s_{1} - s)\| = L\|\mathbf{x}_{n}'\psi'(\tau_{\xi})(\tau_{s_{1}} - \tau_{s})\|, \tag{D.10}$$

where  $\eta \in (\psi(\tau_{s_1}), \psi(\tau_s)), \tau_{\xi} \in (\tau_{s_1}, \tau_s)$  and L is the Lipschitz constant. Since  $||\tau_{s_1} - \tau_s|| \le ||\tau_t - \tau_s|| = O(h_s)$ , the r.h.s. of the above inequation is  $O(h_s)$ .

Besides, by Assumption D.1, we also have

$$\boldsymbol{\epsilon}_{\theta}^{(1)}(\mathbf{x}_s, s) - \frac{\boldsymbol{\epsilon}_{\theta}(\mathbf{x}_{s_1}, s_1) - \boldsymbol{\epsilon}_{\theta}(\mathbf{x}_s, s)}{\phi_1(m)r_1h_s} = O(1) - \frac{O(h_s)}{h_s} = O(1). \tag{D.11}$$

Hence  $\mathbf{x}_t - \tilde{\mathbf{x}}_t = O(h_s^2)$ . We prove that SciRE-Solver-2 is at least a first order solver.

Furthermore, we will prove that **SciRE-Solver-2** is a second order solver under mild condition. Specifically, while  $\phi_1(m) = \phi_1(3) = 2/3$ , by the Lagrange's mean value theorem, there exists  $\xi \in (s_1, s)$  such that

$$\frac{\boldsymbol{\epsilon}_{\theta}\left(\mathbf{x}_{s_{1}}, s_{1}\right) - \boldsymbol{\epsilon}_{\theta}\left(\mathbf{x}_{\xi}, \xi\right)}{\phi_{1}(m)r_{1}h_{s}} = \boldsymbol{\epsilon}_{\theta}^{(1)}\left(\mathbf{x}_{\xi}, \xi\right) + O(h_{s}). \tag{D.12}$$

Note that  $\phi_1(m)r_1h_s = \tau_{s1} - \tau_{\xi}$  and  $(1 - \phi_1(m))r_1h_s = \tau_{\xi} - \tau_s$ , where  $\phi_1(m) = 1/3$ , hence

$$\frac{\boldsymbol{\epsilon}_{\theta}\left(\mathbf{x}_{s_{1}}, s_{1}\right) - \boldsymbol{\epsilon}_{\theta}\left(\mathbf{x}_{s}, s\right)}{\phi_{1}(m)r_{1}h_{s}} = \frac{\boldsymbol{\epsilon}_{\theta}\left(\mathbf{x}_{s_{1}}, s_{1}\right) - \boldsymbol{\epsilon}_{\theta}\left(\mathbf{x}_{\xi}, \xi\right)}{\phi_{1}(m)r_{1}h_{s}} + \frac{\boldsymbol{\epsilon}_{\theta}\left(\mathbf{x}_{\xi}, \xi\right) - \boldsymbol{\epsilon}_{\theta}\left(\mathbf{x}_{s}, s\right)}{\phi_{1}(m)r_{1}h_{s}}$$

$$= \boldsymbol{\epsilon}_{\theta}^{(1)}\left(\mathbf{x}_{\xi}, \xi\right) + O(h_{s}) + \frac{1}{2}\frac{\boldsymbol{\epsilon}_{\theta}\left(\mathbf{x}_{\xi}, \xi\right) - \boldsymbol{\epsilon}_{\theta}\left(\mathbf{x}_{s}, s\right)}{(1 - \phi_{1}(m))r_{1}h_{s}}$$

$$= \boldsymbol{\epsilon}_{\theta}^{(1)}\left(\mathbf{x}_{\xi}, \xi\right) + \frac{1}{2}\boldsymbol{\epsilon}_{\theta}^{(1)}\left(\mathbf{x}_{s}, s\right) + O(h_{s}).$$
(D.13)

Combining the above equation with Eq. (D.9), we have

$$\frac{\mathbf{x}_{t} - \tilde{\mathbf{x}}_{t}}{\alpha_{t}} = \frac{h_{s}^{2}}{2} \boldsymbol{\epsilon}_{\theta}^{(1)} (\mathbf{x}_{s}, s) - \frac{h_{s}^{2}}{2} \frac{\boldsymbol{\epsilon}_{\theta} (\mathbf{x}_{s_{1}}, s_{1}) - \boldsymbol{\epsilon}_{\theta} (\mathbf{x}_{s}, s)}{\phi_{1}(m)r_{1}h_{s}} + O(h_{s}^{3})$$

$$= \frac{h_{s}^{2}}{2} \boldsymbol{\epsilon}_{\theta}^{(1)} (\mathbf{x}_{s}, s) - \frac{h_{s}^{2}}{2} \left( \boldsymbol{\epsilon}_{\theta}^{(1)} (\mathbf{x}_{\xi}, \xi) + \frac{1}{2} \boldsymbol{\epsilon}_{\theta}^{(1)} (\mathbf{x}_{s}, s) \right) + O(h_{s}^{3})$$

$$= \frac{h_{s}^{2}}{4} \left( \boldsymbol{\epsilon}_{\theta}^{(1)} (\mathbf{x}_{s}, s) - 2\boldsymbol{\epsilon}_{\theta}^{(1)} (\mathbf{x}_{\xi}, \xi) \right) + O(h_{s}^{3}),$$
(D.14)

where  $\xi \in (s_1, s)$ . By Assumption D.1,  $\epsilon_{\theta}^{(2)}(\mathbf{x}_s, s)$  is bounded hence the first term in the r.h.s. of above equation is  $O(h_s^3)$ . While for the second term, we find that

$$\begin{aligned}
& \boldsymbol{\epsilon}_{\theta}^{(1)}(\mathbf{x}_{s}, s) - 2\boldsymbol{\epsilon}_{\theta}^{(1)}(\mathbf{x}_{\xi}, \xi) \\
&= \left[ \boldsymbol{\epsilon}_{\theta}^{(1)}(\mathbf{x}_{s}, s) - (1 + \frac{1}{2})\boldsymbol{\epsilon}_{\theta}^{(1)}(\mathbf{x}_{s_{1}}, s_{1}) \right] + \left[ (1 + \frac{1}{2})\boldsymbol{\epsilon}_{\theta}^{(1)}(\mathbf{x}_{s_{1}}, s_{1}) - 2\boldsymbol{\epsilon}_{\theta}^{(1)}(\mathbf{x}_{\xi}, \xi) \right] \\
&= \left[ \boldsymbol{\epsilon}_{\theta}^{(1)}(\mathbf{x}_{s}, s) - (1 + \frac{1}{4})\boldsymbol{\epsilon}_{\theta}^{(1)}(\mathbf{x}_{\xi}, \xi) \right] + \left[ (1 + \frac{1}{4})\boldsymbol{\epsilon}_{\theta}^{(1)}(\mathbf{x}_{\xi}, \xi) - (1 + \frac{1}{2})\boldsymbol{\epsilon}_{\theta}^{(1)}(\mathbf{x}_{s_{1}}, s_{1}) \right] \\
&+ \left[ (1 + \frac{1}{2})\boldsymbol{\epsilon}_{\theta}^{(1)}(\mathbf{x}_{s_{1}}, s_{1}) - (1 + \frac{1}{2} + \frac{1}{4})\boldsymbol{\epsilon}_{\theta}^{(1)}(\mathbf{x}_{s}, s) \right] + \left[ (1 + \frac{1}{2} + \frac{1}{4})\boldsymbol{\epsilon}_{\theta}^{(1)}(\mathbf{x}_{s}, s) - 2\boldsymbol{\epsilon}_{\theta}^{(1)}(\mathbf{x}_{\xi}, \xi) \right] \end{aligned}$$
(D.15)

22

We now define *group*, for example,  $\epsilon_{\theta}^{(1)}(\mathbf{x}_s, s) - (1 + \frac{1}{2})\epsilon_{\theta}^{(1)}(\mathbf{x}_{s_1}, s_1)$ , which is grouped by "[]". We also find that for each group, if the coefficient of the first term is l, then the coefficient of the second term is  $l + \frac{1}{2^n}$  after using dichotomy for n times. Note that  $l \in [1, 2)$  such that  $l + \frac{1}{2^n} \in (1, 2]$ ,  $\forall n \in \mathbb{N}$ . Besides, t takes two different values in  $\{s, s_1, \xi\}$ . By Eq. (D.10) and Assumption D.3, if n is large enough, each group is  $O(h_s)$ , for example,

$$l\boldsymbol{\epsilon}_{\theta}^{(1)}\left(\mathbf{x}_{s_{1}},s_{1}\right)-\left(l+\frac{1}{2^{n}}\right)\boldsymbol{\epsilon}_{\theta}^{(1)}\left(\mathbf{x}_{s},s\right)=l\boldsymbol{\epsilon}_{\theta}^{(1)}\left(\mathbf{x}_{s_{1}},s_{1}\right)-l\boldsymbol{\epsilon}_{\theta}^{(1)}\left(\mathbf{x}_{\rho},\rho\right)=O(h_{s}). \tag{D.16}$$

Hence  $\epsilon_{\theta}^{(1)}(\mathbf{x}_s, s) - 2\epsilon_{\theta}^{(1)}(\mathbf{x}_{\xi}, \xi)$  is  $O(2^n h_s)$ . In practice, n is finite, meaning that  $2^n$  is bounded and  $O(2^n h_s) = O(h_s)$ . Subquently, the proof is completed by

$$\frac{\mathbf{x}_t - \tilde{\mathbf{x}}_t}{\alpha_t} = O(h_s^3) + \frac{h_s^2}{4}O(h_s) + O(h_s^3) = O(h_s^3). \tag{D.17}$$

#### **D.3** Proof of Theorem 3.2 when k = 3

In this subsection, we prove the global convergence order of SciRE-Solver-3 is no less than 2. *Proof.* For each iteration step, we first update according to:

$$h_s = \tau_t - \tau_s, \tag{D.18}$$

$$s_1 = \psi(\tau_s + r_1 h_s),\tag{D.19}$$

$$s_2 = \psi(\tau_s + r_2 h_s),\tag{D.20}$$

$$\mathbf{u}_{1} = \frac{\alpha_{s_{1}}}{\alpha_{s}} \mathbf{x}_{s} + \alpha_{s_{1}} r_{1} h_{s} \boldsymbol{\epsilon}_{\theta} \left( \mathbf{x}_{s}, s \right), \tag{D.21}$$

$$\mathbf{u}_{2} = \frac{\alpha_{s_{2}}}{\alpha_{s}} \mathbf{x}_{s} + \alpha_{s_{2}} r_{2} h_{s} \boldsymbol{\epsilon}_{\theta} \left( \mathbf{x}_{s}, s \right) + \alpha_{s_{2}} \frac{h_{s}}{\phi_{1}(m)} \left( \boldsymbol{\epsilon}_{\theta} \left( \mathbf{u}_{1}, s_{1} \right) - \boldsymbol{\epsilon}_{\theta} \left( \mathbf{x}_{s}, s \right) \right), \tag{D.22}$$

$$\tilde{\mathbf{x}}_{t} = \frac{\alpha_{t}}{\alpha_{s}} \mathbf{x}_{s} + \alpha_{t} h_{s} \boldsymbol{\epsilon}_{\theta} \left( \mathbf{x}_{s}, s \right) + \alpha_{t} \frac{h_{s}^{2}}{2\phi_{1}(m) r_{2} h_{s}} \left( \boldsymbol{\epsilon}_{\theta} \left( \mathbf{u}_{2}, s_{2} \right) - \boldsymbol{\epsilon}_{\theta} \left( \mathbf{x}_{s}, s \right) \right), \tag{D.23}$$

where  $\tilde{\mathbf{x}}_t$  denotes the approximate solution of  $\mathbf{x}_t$  computed by SciRE-Solver-3,  $r_1 \in (0, 1)$  and  $r_2 = 1 - r_1$  are hyperparameters so that  $s_1, s_2 \in (t, s)$ . We firstly prove that  $\mathbf{u}_2 - \mathbf{x}_{s_2} = O(h_s^3)$ :

$$\mathbf{u}_{2} = \frac{\alpha_{s_{2}}}{\alpha_{s}} \mathbf{x}_{s} + \alpha_{s_{2}} r_{2} h_{s} \boldsymbol{\epsilon}_{\theta} \left( \mathbf{x}_{s}, s \right) + \alpha_{s_{2}} \frac{h_{s}}{\phi_{1}(m)} \left( \boldsymbol{\epsilon}_{\theta} \left( \mathbf{u}_{1}, s_{1} \right) - \boldsymbol{\epsilon}_{\theta} \left( \mathbf{x}_{s}, s \right) \right)$$

$$= \underbrace{\frac{\alpha_{s_{2}}}{\alpha_{s}} \mathbf{x}_{s} + \alpha_{s_{2}} r_{2} h_{s} \boldsymbol{\epsilon}_{\theta} \left( \mathbf{x}_{s}, s \right) + \alpha_{s_{2}} \frac{h_{s}}{\phi_{1}(m)} \left( \boldsymbol{\epsilon}_{\theta} \left( \mathbf{x}_{s_{1}}, s_{1} \right) - \boldsymbol{\epsilon}_{\theta} \left( \mathbf{x}_{s}, s \right) \right) + O(h_{s}^{3}),$$

$$\underbrace{\boldsymbol{\kappa}_{s_{2}}} \left( \mathbf{x}_{s} + \alpha_{s_{2}} r_{2} h_{s} \boldsymbol{\epsilon}_{\theta} \left( \mathbf{x}_{s}, s \right) + \alpha_{s_{2}} \frac{h_{s}}{\phi_{1}(m)} \left( \boldsymbol{\epsilon}_{\theta} \left( \mathbf{x}_{s_{1}}, s_{1} \right) - \boldsymbol{\epsilon}_{\theta} \left( \mathbf{x}_{s}, s \right) \right) + O(h_{s}^{3}),$$

$$\underbrace{\boldsymbol{\kappa}_{s_{2}}} \left( \mathbf{x}_{s} + \alpha_{s_{2}} r_{2} h_{s} \boldsymbol{\epsilon}_{\theta} \left( \mathbf{x}_{s}, s \right) + \alpha_{s_{2}} \frac{h_{s}}{\phi_{1}(m)} \left( \boldsymbol{\epsilon}_{\theta} \left( \mathbf{x}_{s_{1}}, s_{1} \right) - \boldsymbol{\epsilon}_{\theta} \left( \mathbf{x}_{s}, s \right) \right) + O(h_{s}^{3}),$$

$$\underbrace{\boldsymbol{\kappa}_{s_{2}}} \left( \mathbf{x}_{s} + \alpha_{s_{2}} r_{2} h_{s} \boldsymbol{\epsilon}_{\theta} \left( \mathbf{x}_{s}, s \right) + \alpha_{s_{2}} \frac{h_{s}}{\phi_{1}(m)} \left( \boldsymbol{\epsilon}_{\theta} \left( \mathbf{x}_{s_{1}}, s_{1} \right) - \boldsymbol{\epsilon}_{\theta} \left( \mathbf{x}_{s}, s \right) \right) + O(h_{s}^{3}),$$

$$\underbrace{\boldsymbol{\kappa}_{s_{2}}} \left( \mathbf{x}_{s} + \alpha_{s_{2}} r_{2} h_{s} \boldsymbol{\epsilon}_{\theta} \left( \mathbf{x}_{s}, s \right) + \alpha_{s_{2}} \frac{h_{s}}{\phi_{1}(m)} \left( \boldsymbol{\epsilon}_{\theta} \left( \mathbf{x}_{s_{1}}, s_{1} \right) - \boldsymbol{\epsilon}_{\theta} \left( \mathbf{x}_{s}, s \right) \right) + O(h_{s}^{3}),$$

by  $\mathbf{u}_1 - \mathbf{x}_{s_1} = O(h_s^2)$  and Assumption D.2.

Next, taking n = 2 in Eq. (D.3), we can get the exact solution of  $\mathbf{x}_t$  as follows:

$$\mathbf{x}_{t} = \frac{\alpha_{t}}{\alpha_{s}} \mathbf{x}_{s} + \alpha_{t} h_{s} \boldsymbol{\epsilon}_{\theta} \left( \mathbf{x}_{s}, s \right) + \alpha_{t} \sum_{k=1}^{2} \frac{h_{s}^{k+1}}{(k+1)!} \boldsymbol{\epsilon}_{\theta}^{(k)} \left( \mathbf{x}_{s}, s \right) + O(h_{s}^{4})$$
(D.25)

Then by subtracting the last equation from Eq. (D.23) and using  $\mathbf{u}_1 - \mathbf{x}_{s_1} = O(h_s^2)$ , we have

$$\frac{\mathbf{x}_{t} - \tilde{\mathbf{x}}_{t}}{\alpha_{t}} = \sum_{k=1}^{2} \frac{h_{s}^{k+1}}{(k+1)!} \boldsymbol{\epsilon}_{\theta}^{(k)}(\mathbf{x}_{s}, s) - \frac{h_{s}^{2}}{2\phi_{1}(m)r_{2}h_{s}} (\boldsymbol{\epsilon}_{\theta}(\mathbf{u}_{2}, s_{2}) - \boldsymbol{\epsilon}_{\theta}(\mathbf{x}_{s}, s)) + O(h_{s}^{4}) 
= \frac{h_{s}^{2}}{2} \boldsymbol{\epsilon}_{\theta}^{(1)}(\mathbf{x}_{s}, s) + \frac{h_{s}^{3}}{3!} \boldsymbol{\epsilon}_{\theta}^{(2)}(\mathbf{x}_{s}, s) - \frac{h_{s}^{2}}{2} \frac{\boldsymbol{\epsilon}_{\theta}(\mathbf{x}_{s_{2}}, s_{2}) - \boldsymbol{\epsilon}_{\theta}(\mathbf{x}_{s}, s)}{\phi_{1}(m)r_{2}h_{s}} + O(h_{s}^{4}),$$
(D.26)

where  $\|\boldsymbol{\epsilon}_{\theta}(\mathbf{u}_2, s_2) - \boldsymbol{\epsilon}_{\theta}(\mathbf{x}_{s_2}, s_2)\| = O(\|\mathbf{u}_2 - \mathbf{x}_{s_2}\|) = O(h_s^3)$ . Similar to the proof in D.2, we have

$$\frac{\mathbf{x}_{t} - \tilde{\mathbf{x}}_{t}}{\alpha_{t}} = \sum_{k=1}^{2} \frac{h_{s}^{k+1}}{(k+1)!} \boldsymbol{\epsilon}_{\theta}^{(k)} (\mathbf{x}_{s}, s) - \frac{h_{s}^{2}}{2} \frac{\boldsymbol{\epsilon}_{\theta} (\mathbf{x}_{s_{2}}, s_{2}) - \boldsymbol{\epsilon}_{\theta} (\mathbf{x}_{s}, s)}{\phi_{1}(m) r_{2} h_{s}} + O(h_{s}^{4})$$

$$= \frac{h_{s}^{3}}{3!} \boldsymbol{\epsilon}_{\theta}^{(2)} (\mathbf{x}_{s}, s) + \frac{h_{s}^{2}}{2} \boldsymbol{\epsilon}_{\theta}^{(1)} (\mathbf{x}_{s}, s) - \frac{h_{s}^{2}}{2} \left(\boldsymbol{\epsilon}_{\theta}^{(1)} (\mathbf{x}_{\xi}, \xi) + \frac{1}{2} \boldsymbol{\epsilon}_{\theta}^{(1)} (\mathbf{x}_{s}, s)\right) + O(h_{s}^{3})$$

$$= \frac{h_{s}^{3}}{3!} \boldsymbol{\epsilon}_{\theta}^{(2)} (\mathbf{x}_{s}, s) + \frac{h_{s}^{2}}{4} \left(\boldsymbol{\epsilon}_{\theta}^{(1)} (\mathbf{x}_{s}, s) - 2\boldsymbol{\epsilon}_{\theta}^{(1)} (\mathbf{x}_{\xi}, \xi)\right) + O(h_{s}^{3})$$

$$= O(h_{s}^{3}) + 2^{n} O(h_{s}^{3}) + O(h_{s}^{3}) = O(h_{s}^{3}),$$
(D.27)

where  $\xi \in (s_2, s)$  and  $n \in \mathbb{N}$  is finite. Hence we prove that the global convergence order of SciRE-Solver-3 is no less than 2.

## **Appendix E Experiment Details**

In this section, we provide more details on SciRE-Solver and further demonstrate the performance of SciRE-Solver on both discrete-time DPMs and continuous-time DPMs. Specifically, we consider the 1000-step DPMs [2] and the 4000-step DPMs [19], and consider the end time  $\epsilon$  and time trajectory for sampling. We test our method for sampling the most widely-used variance-preserving (VP) type DPMs [1, 3]. In this case, we have  $\alpha_t^2 + \sigma_t^2 = 1$  for all  $t \in [0, T]$ . In spite of this, our method and theoretical results are general and independent of the choice of the noise schedule  $\alpha_t$  and  $\sigma_t$ . For all experiments, we evaluate SciRE-Solver on NVIDIA TITAN X GPUs.

#### E.1 End Time of Sampling

Theoretically, we need to solve diffusion ODEs from time T to time 0 to generate samples. Practically, the training and evaluation for the noise prediction model  $\epsilon_{\theta}(\mathbf{x}_t,t)$  usually start from time T to time  $\epsilon$  to avoid numerical issues for t near to 0, where  $\epsilon \geq 0$  is a hyperparameter [3]. In contrast to the sampling methods based on diffusion SDEs [2, 3], we, like DPM-Solver [13], do not incorporate the "denoising" trick (i.e., setting the noise variance to zero) in the final step at time  $\epsilon$ . Instead, we solely solve diffusion ODEs from T to  $\epsilon$  using the SciRE-Solver.

#### **E.2** Time trajectories

Let  $\{t_i\}_{i=0}^N$  be the time trajectory of diffusion probabilistic models, where  $t_N = T$  and  $t_0 = \epsilon \ge 0$ . In the context of fast sampling, it is always desirable for the number N of time points in the time trajectory to be as small as possible. However, the selection of the optimal time trajectory remains an open problem for the few-step sampling regime of diffusion probabilistic models. In this work, we hypothesize that selecting a time trajectory with sparser time points in the middle and relatively denser time points at the two ends would be beneficial for improving the quality of sample generation. To validate this hypothesis, inspired by the logarithmic and sigmoid functions, we propose two parametrizable alternative methods for the NSR function to compute the time trajectory, named as NSR-type and Sigmoid-type time trajectories, respectively.

**NSR-type:** For a given starting time  $t_T$  and ending time  $t_0$  of the sampling, the time values at the intermediate endpoints  $t_i$  of NSR-type time trajectory are obtained as follows:

- 1.  $trans_T = -\log(NSR(t_T) + k \cdot NSR(t_0)),$
- 2.  $trans_0 = -\log(NSR(t_0) + k \cdot NSR(t_0)),$
- 3.  $trans_i = trans_T + i \cdot \frac{trans_0 trans_T}{N}$ ,
- 4.  $t_i = \text{rNSR}(e^{-\text{trans}_i} k \cdot \text{NSR}(t_0)),$

where k is a hyperparameter that controls the flexibility of NSR-type time trajectory.

In all our experiments, we found that relatively good results can be obtained when  $k \in [2, 7]$ . This means that when using this kind of time trajectory, one can consider setting the value of k within this range.

**Sigmoid-type:** For a given starting time  $t_T$  and ending time  $t_0$  of the sampling, the time values at the intermediate endpoints  $t_i$  of **Sigmoid-type** time trajectory are obtained as follows:

1. 
$$trans_T = -\log(NSR(t_T))$$
,  $trans_0 = -\log(NSR(t_0))$ ,

```
2. central = k \cdot \text{trans}_T + (1 - k) \cdot \text{trans}_0,
```

- 3.  $shift_T = trans_T central$ ,  $shift_0 = trans_0 central$ ,
- 4.  $scale = shift_T + shift_0$ ,
- $$\begin{split} &5. & \text{sigm}_T = sigmoid\left(\frac{\text{shift}_T}{\text{scale}}\right), \text{ sigm}_0 = sigmoid\left(\frac{\text{shift}_0}{\text{scale}}\right), \\ &6. & \text{sigm}_i = \text{sigm}_T + i \cdot \frac{\text{sigm}_0 \text{sigm}_T}{N}, \end{split}$$
- 7.  $trans_i = scale \cdot logistic(sigm_i) + central,$
- 8.  $t_i = \text{rNSR}(e^{-\text{trans}_i}),$

where k is a hyperparameter that controls the flexibility of Sigmoid-type time trajectory.

Empirically, we suggest using the NSR-type time trajectory. However, when NFE is less than or equal to 15, it is recommended to try using the Sigmoid-type time trajectory. The generation quality measured by FID of NSR-type time trajectory and Sigmoid-type time trajectory are shown in Tab. (6) and Tab. (5), respectively. Besides, we also demonstrate the efficiency of our proposed algorithms by using conventional time-quadratic trajectory in Tab. (4). In these experimental results, NSR-type time trajectory is better than time-quadratic trajectory.

#### E.3 Comparing sample quality with different samplers

We show the detailed FID results of different sampling methods for DPMs on CIFAR-10 and CelebA 64×64 with discrete-time or continuous-time pre-trained models in Table 1. We utilize the code and checkpoint provided in [2, 3, 19]. Specifically, we employ their *checkpoint\_8* of the "VP deep" type. In this table, we compare the FID achieved by our proposed SciRE-Solver with the best FID reported in existing literature at the same NFE. We consistently use the NSR-type time trajectory with parameter k = 3.1 for SciRE-Solver on the discrete models of CIFAR-10 and CelebA 64×64 datasets. For continuous models on the CIFAR-10 dataset, we use a Sigmoid-type time trajectory with parameter k = 0.65 for the SciRE-Solver when the NFE is less than 15. When NFE is greater than or equal to 15, we consistently use an NSR-type time trajectory with k = 3.1. In order to objectively compare the quality of generated samples for the CelebA 64×64 dataset, given the presence of different FID statistical data, we utilized the FID stats employed by Liu et al. [24] in Tables 1, 4 and 6, and utilized the FID stats employed by Lu et al. [13] in Tables 2 and 7. Fig. 3 illustrates the FIDs achieved by different samplers at various NFE levels. Moreover, in Table 3, we also evaluate SciRE-Solver, DPM-Solver and DDIM with the same codebase and settings on the pre-trained model of high-resolution ImageNet 128×128 dataset [4], refer to Figures 6 and 7 for a comparison of samples under this scenario. In all tables, the results † means the actual NFE is smaller than the given NFE in the table.

In Table 2, in order to ensure fairness, we compare the generation performance of SciRE-Solver with DPM-Solver and DDIM on discrete models [2, 14] of CIFAR-10 and CelebA 64×64 datasets using the same trajectories, settings and codebase. In this experiment, we employ different time trajectories to evaluate the sampling performance of each sampling algorithm, such as the NSR trajectory and the logNSR trajectory [13]. Unlike in Table 1 with parameter k = 3.1, we consistently use parameter k = 2 for the NSR time trajectory in Table 2, in order to showcase the impact of different k values on the samplers. Meanwhile, we also compare the performance of generative samples for these three samplers at different sampling endpoints, such as 1e - 3 and 1e - 4.

Tables 1 and 2 demonstrate that the SciRE-Solver attains SOTA sampling performance with limited NFE on both discrete-time and continuous-time DPMs in comparison to existing training-free sampling algorithms. Such as, in Table 1, we achieve 3.48 FID with 12 NFE and 2.42 FID with 20 NFE for continuous-time DPMs on CIFAR10, respectively. Furthermore, with fewer NFE, SciRE-Solver surpass the benchmark values demonstrated in the original paper of the proposed pre-trained model. For example, we reach SOTA value of 2.40 FID with no more than 100 NFE for continuous-time DPMs and of 3.15 FID with 84 NFE for discrete-time DPMs on CIFAR-10, as well as of 2.17 FID with 18 NFE for discrete-time DPMs on CelebA 64×64. Moreover, SciRE-Solver can also achieve SOTA sampling performance within 100 NFE for both the NSR time trajectory with different parameter values k and the logSNR time trajectory, as shown in Tables 1 and 2. Especially, in Table 2, DPM-Solver is more likely to achieve better sampling performance within 15 NFE for the logSNR time trajectory and the NSR time trajectory with k = 2. However, when NFE exceeds 15, ScrRE-Solver becomes more advantageous. Moreover, when the endpoint of the sampling is set at 1e - 4, both with the logSNR time trajectory and NSR time trajectory (k = 2), SciRE-Solver can achieve SOTA sampling performance between 50 NFE and 100 NFE.

In Table 3, we also evaluate SciRE-Solver, DPM-Solver and DDIM on the high-resolution ImageNet 128×128 dataset [4]. For the sake of fairness, we use the same uniform time trajectory, the same codebase, and the same settings to evaluate SciRE-Solver-2, DPM-Solver-2, and DDIM for 10, 12, 15, 20, and 50 NFEs. The numerical experiment results report that SciRE-Solver-2 achieved 5.58 FID with 10 NFE and 3.67 FID with 20 NFE, respectively, while DMP-Solver-2 only achieved 4.17 FID with 50 NFE. In all these different NFEs, SciRE-Solver-2 outperforms DPM-Solver-2. In summary, within 20 NFE, SciRE-Solver with NSR trajectory (k = 3.1) achieves better FID than existing training-free solvers [33, 14, 28, 13, 24, 25] for CIFAR-10 and CelebA 64×64 datasets, as shown Table 1. Meanwhile, within 100 NFE (or even 1000 NFE), existing solvers in the context of discrete models on CIFAR-10 dataset are hardly able to achieve an FID below 3.45, as shown in Table 1. On the other hand, SciRE-Solver, with different time trajectories such as logNSR trajectory and NSR trajectory, can achieve an FID below 3.17, and even surpass the 3.16 FID obtained by DDPM at 1000 NFE, as shown in Tables 1 and 2. For the continuous VP-type model on CIFAR-10, SciRE-Solver also surpasses the 2.41 FID obtained by Song et al. [3] using SDE solver with 1000 NFE. In Table 2, under the time trajectories, settings and the same codebase, SciRE-Solver outperforms the DPM-Solver [13] widely used in stable diffusion [34]. Specifically, SciRE-Solver achieves an FID of 3.16 and 2.03 within 100 NFE on CIFAR-10 and CelebA 64×64 datasets respectively, whereas DPM-Solver struggles to achieve FID values lower than 3.50 and 2.79 respectively on the same datasets. Furthermore, the FID comparison on the high-resolution 128×128 dataset presented in Table 3 suggests that SciRE-Solver also possesses advantages in sample generation tasks involving high-resolution image datasets. For more random sampling sample comparisons on different highresolution ( $\geq 128 \times 128$ ) image datasets, please refer to Figures 6, 7, 8, 12, 13, 14, and 15.

#### E.4 Ablations study

#### Different orders and Starting times E.4.1

**Order** We compare the sample quality with different orders of SciRE-Solver-2,3. However, in practice, the actual NFE may be smaller than the given NFE, for example, given the NFE=15, the actucal NFE of SciRE-Solver-2 is 14. To mitigate this problem, we propose the SciRE-Solver-agile method for continuous models. We compare the results of models with different orders on CIFAR-10 and CelebA 64×64 datasets. Our results indicate that if NFE is less than 20, SciRE-Solver-2 outperforms SciRE-Solver-3, or the latter variant is superior – depending on the specific use case.

Starting time We also compare SciRE-Solver-2,3 with different starting times  $\epsilon = 10^{-3}$  and  $\epsilon = 10^{-4}$ . Corresponding results are placed in Tab. 4 and Tab. (6). We use time-quadratic trajectory and NSR-type time trajectory for both SciRE-Solver-2 and SciRE-Solver-3 on CIFAR-10 and CelebA 64 × 64 datasets. In our study on the CIFAR-10 dataset, we have observed that employing a sampling method with  $\epsilon = 10^{-3}$  results in superior sample quality for both continuous and discrete models when NFE is restricted to either 12 or 15. However, for NFE values greater than 15, we recommend opting for  $\epsilon = 10^{-4}$  to ensure the generation of high-quality samples. Moreover, in our analysis of the CelebA 64 ×64 dataset, we have found that  $\epsilon = 10^{-4}$  consistently yields better results than  $\epsilon = 10^{-3}$  across different orders and NFEs. It is noteworthy that for NFE=20, SciRE-Solvers-2,3 show promising results that are on par with the former.

## E.4.2 Comparison between the Using of RDE Method and Non-RDE

We use FID to measure the sampling performance of the sampling algorithms when estimating derivatives using finite difference estimation (FDE) and recursive derivative estimation (RDE), respectively. Here, we set  $\phi_1(m) = 1$  in SciRE-Solver to represent the sampling algorithm based on FDE method. Based on the FID metric of generated samples, with the same codebase, we assess the performance of these two derivative estimation methods using discrete diffusion models trained on the CIFAR-10 and CelebA 64×64 datasets. Without loss of generality, we use a consistent NSR trajectory with k = 2, because SciRE-Solver can achieve the better quality of generated samples for  $k \in [2, 7]$ , as mentioned in Section E.2. Our numerical experiments demonstrate that, across different initial times, the quality of generated samples achieved by the SciRE-Solver using RDE evaluation consistently outperforms that of the solver obtained through FDE evaluation, as shown in Table 7.

**E.4.3** 
$$\phi_1(m) = \phi_1(3)$$
 or  $\phi_1(m) = \frac{e-1}{2}$ 

**E.4.3**  $\phi_1(m) = \phi_1(3)$  or  $\phi_1(m) = \frac{e-1}{e}$  When running our proposed SciRE-Solver-k in Algorithm 1 and Algorithm 2, it is necessary to assign a value m to  $\phi_1(m)$ . As stated in Corollary 1, when assigning m, we need to ensure that  $m \ge 3$ . Considering that the limit of  $\phi_1(m)$  is  $\frac{e-1}{e}$ , i.e.,  $\lim_{m \to \infty} \phi_1(m) = \lim_{m \to \infty} \sum_{k=1}^m \frac{(-1)^{k-1}}{k!} = \frac{e-1}{e}$ , then

Table 2: Generation quality measured by FID  $\downarrow$  of different sampling methods for DPMs on the pre-trained discrete-time models [2, 14] of CIFAR-10 and CelebA 64×64.

Trajectory	Initial Time	Sampling method \NFE	12	15	20	50	100
CIFAR-10 (di	screte-time mo	del [2], linear noise schedu	le)				
		DDIM [14]	16.08	12.43	9.28	5.36	4.55
1 CNID[12]	10-3	DPM-Solver-2 [13]	5.18	†4.42	4.05	3.97	3.97
logSNR[13]	$\epsilon = 10^{-3}$	DPM-Solver-3 [13]	7.39	4.60	†4.33	†3.98	†3.97
		SciRE-Solver-2 (ours)	5.48	†4.55	3.96	3.66	3.71
		SciRE-Solver-3 (ours)	8.53	5.00	†4.34	†3.66	†3.62
		DDIM [14]	17.40	13.12	9.54	5.03	4.13
logCND[12]	10-4	DPM-Solver-2 [13]	6.40	†5.26	4.02	3.56	3.51
logSNR[13]	$\epsilon = 10^{-4}$	DPM-Solver-3 [13]	9.52	5.17	† <b>3.80</b>	†3.53	†3.50
		SciRE-Solver-2 (ours)	6.48	†5.35	4.01	3.34	3.27
		SciRE-Solver-3 (ours)	11.71	5.99	†4.15	†3.30	†3.163
		DDIM [14]	13.58	10.63	8.12	5.03	4.40
NSR (k = 2)	$\epsilon = 10^{-3}$	DPM-Solver-2 [13]	4.91	†4.51	4.19	4.00	3.96
NSK(k-2)	$\epsilon = 10^{\circ}$	DPM-Solver-3 [13]	7.33	4.97	†4.56	†4.00	†3.96
		SciRE-Solver-2 (ours)	4.49	†4.12	3.74	3.70	3.76
		SciRE-Solver-3 (ours)	5.29	4.19	†3.94	†3.76	†3.71
		DDIM [14]	15.51	11.86	8.77	4.86	4.07
NSR (k = 2)	$\epsilon = 10^{-4}$	DPM-Solver-2 [13]	5.38	†4.46	3.78	3.53	3.51
NSK (k = 2)	$\epsilon = 10^{\circ}$	DPM-Solver-3 [13]	7.29	4.03	† <b>3.66</b>	†3.52	†3.50
		SciRE-Solver-2 (ours)	5.91	†4.76	3.88	3.30	3.28
G 1 1 4 64 6	4 / 1	SciRE-Solver-3 (ours)	9.10	4.52	†4.07	†3.24	†3.167
CelebA 64×64	1 (discrete-time	e model [14], linear noise s					
		DDIM [14]	14.37	11.91	9.66	6.13	5.15
logSNR[13]	$\epsilon = 10^{-3}$	DPM-Solver-2 [13]	3.952	†3.953	4.05	4.21	4.24
10g5141(13]	E - 10	DPM-Solver-3 [13]	3.79	3.91	†4.05	†4.26	†4.25
		SciRE-Solver-2 (ours)	5.39	†4.51	3.76	3.49	3.71
		SciRE-Solver-3 (ours)	4.91	3.65	†3.29	†3.09	†3.41
		DDIM [14]	12.81	10.28	7.98	4.52	3.59
logSNR[13]	$\epsilon = 10^{-4}$	DPM-Solver-2 [13]	3.26	†3.14	2.92	2.82	2.82
logorik[13]	$\epsilon = 10$	DPM-Solver-3 [13]	3.93	2.91	†2.85	†2.82	†2.81
		SciRE-Solver-2 (ours)	4.29	†3.70	2.87	2.37	2.43
		SciRE-Solver-3 (ours)	5.04	3.43	†2.58	<sup>†</sup> 2.06	<sup>†</sup> 2.20
		DDIM [14]	13.08	10.99	8.96	5.88	4.40
NSR (k = 2)	$\epsilon = 10^{-3}$	DPM-Solver-2 [13]	5.39	†4.93	4.37	4.24	4.236
NSR (k = 2)	e – 10	DPM-Solver-3 [13]	6.14	4.77	†4.41	†4.24	†4.24
		SciRE-Solver-2 (ours)	4.61	†4.20	3.58	3.56	3.76
		SciRE-Solver-3 (ours)	4.75	3.33	†3.04	†3.15	†3.51
		DDIM [14]	11.88	9.59	7.53	4.38	3.54
NSR (k = 2)	$\epsilon = 10^{-4}$	DPM-Solver-2 [13]	3.11	†2.91	2.88	2.79	2.81
NSIX (K - 2)	$\epsilon = 10^{\circ}$	DPM-Solver-3 [13]	2.94	2.88	†2.87	†2.80	†2.81
		SciRE-Solver-2 (ours)	3.95	†3.39	2.61	2.31	2.43
		SciRE-Solver-3 (ours)	4.47	2.68	†2.29	†2.03	<sup>†</sup> 2.20

Table 3: Generation quality measured by FID  $\downarrow$  of different sampling methods with the same codebase for DPMs on the pre-trained discrete-time model of Imagenet 128×128 [4].

Trajectory	Initial Time	Sampling method \NFE	10	12	15	20	50
Imagenet 128×128 [4] (with classifier guidance: scale=1.25, under the same codebase)							
Uniform time [2]	$\epsilon = 10^{-3}$	DDIM [14] DPM-Solver-2 [13]	9.33 10.17		6.07 †6.68	4.91 5.46	
	C 10	SciRE-Solver-2 (our)			†4.27		

T-1-1- 4.	CaiDE Ca	1	time-quadratic	4:
Table 4.	OCINE-OU	ivei willi	time-duadratic	ualectory

					•	
Initial time	Sampling method \ NFE	12	15	20	50	100
CIFAR-10 (d	discrete-time model [2])					
$\epsilon = 10^{-3}$	SciRE-Solver-2	4.86	<sup>†</sup> 4.10	3.56	3.74	3.83
C = 10	SciRE-Solver-3	19.37	11.18	†7.48	†3.94	†3.85
$\epsilon = 10^{-4}$	SciRE-Solver-2	6.13	<sup>†</sup> 5.12	3.83	3.31	3.27
$\epsilon = 10$	SciRE-Solver-3	22.39	13.09	†8.54	†3.45	†3.22
CIFAR-10 (	VP deep continuous-time me	odel [3])				
	SciRE-Solver-2	5.00	†4.24	3.23	2.59	2.53
$\epsilon = 10^{-4}$	SciRE-Solver-3	12.53	7.33	<sup>†</sup> 5.43	†2.64	† <b>2.50</b>
$\epsilon = 10^{-4}$	SciRE-Solver-agile	5.03	4.24	3.21	2.59	2.51
Initial time	Sampling method \ NFE	12	15	20	30	50
CelebA 64×	64 (discrete-time model[14]	)				
c = 10 <sup>-3</sup>	SciRE-Solver-2	5.83	†4.67	3.92	3.77	3.86
$\epsilon = 10^{-3}$	SciRE-Solver-3	8.72	5.06	†3.81	†3.31	†3.56
$\epsilon = 10^{-4}$	SciRE-Solver-2	4.24	†3.27	2.46	2.23	2.20
$\epsilon = 10$	SciRE-Solver-3	11.08	5.62	†3.53	† <b>2.13</b>	† <b>2.03</b>

Table 5: Comparison between different time trajectories, starting time is 1e - 3.

CIFAR-10 (VP deep continuous-time model [3])

CIFAR-10 (VP deep continuous-time model [3])						
Sampling method	Sampling method\ NFE	12	15			
SciRE-Solver-3	NSR-type( $k = 3.2 - 0.005$ ·NFE) Sigmoid-type ( $k = 0.65$ )	4.41 <b>3.48</b>	<b>3.06</b> 3.47			

Table 6: SciRE-Solver with	NSR trajectory	r(k = 3.1).
----------------------------	----------------	-------------

Initial time	Sampling method \ NFE	12	15	20	50	100
CIFAR-10 (discrete-time model [2])						
$\epsilon = 10^{-3}$	SciRE-Solver-2	4.41	†4.09	<b>3.67</b> †3.72	3.70 †3.84	3.80 †3.77
	SciRE-Solver-3	4.68	4.00	3.12	3.84	3.11
$\epsilon = 10^{-4}$	SciRE-Solver-2	5.86	†4.77	3.87	3.28	3.27
ε = 10	SciRE-Solver-3	8.28	4.51	†3.96	†3.23	†3.17
Initial time	Sampling method \ NFE	12	15	20	30	50
CIFAR-10 (	VP deep continuous-time me	odel [3]	)			
	SciRE-Solver-2	5.49	†4.19	3.02	2.55	2.47
$\epsilon = 10^{-4}$	SciRE-Solver-3	6.29	3.39	†2.68	†2.56	<sup>†</sup> 2.44
	SciRE-Solver-2 <b>5.49</b> $^{\dagger}$ 4.19 3.02 2. = $10^{-4}$ SciRE-Solver-3 6.29 <b>3.39</b> $^{\dagger}$ 2.68 $^{\dagger}$ 2.	2.52	2.48			
CelebA 64×	64 (discrete-time model[14]	)				
s - 10-3	SciRE-Solver-2	4.79	†4.28	3.86	3.69	3.82
$\epsilon = 10^{-3}$	SciRE-Solver-3	5.01	3.32	†3.12	†3.09	†3.40
s - 10-4	SciRE-Solver-2	3.91	†3.38	2.56	2.41	2.30
$\epsilon = 10^{-4}$	SciRE-Solver-3	4.07	2.53	† <b>2.17</b>	† <b>2.03</b>	<sup>†</sup> 2.02

Table 7: Comparison of Quality Generation between FDE-based and RDE-based Algorithms. We use consistent NSR trajectory (k=2) and the same codebase.

FDE or RDE	Initial time\ NFE	12	15	20	50	100			
The discrete-time model	The discrete-time model of CIFAR-10 dataset [2]								
FDE (Solver-2)	1e - 3	7.00	†6.00	4.76	4.10	4.03			
	1e - 4	9.03	†7.10	5.05	3.71	3.57			
RDE (SciRE-Solver-2)	1e - 3 1e - 4	<b>4.49</b> 5.91	† <b>4.12</b> †4.76	<b>3.74</b> 3.88	3.70 3.30	3.76 3.28			
FDE (Solver-3)	1e - 3	6.91	5.25	†4.67	†4.04	†4.02			
	1e - 4	10.19	6.12	†5.03	†3.56	†3.52			
RDE (SciRE-Solver-3)	1e - 3	5.29	4.19	†3.94	†3.76	†3.71			
	1e - 4	9.10	4.52	†4.07	† <b>3.24</b>	† <b>3.17</b>			
The discrete-time model	of CelebA 64×64 da	ataset [2]							
FDE (Solver-2)	1e - 3	7.82	†6.87	5.48	4.48	4.33			
	1e - 4	7.04	†5.87	4.17	3.05	2.89			
RDE (SciRE-Solver-2)	1e - 3	4.67	†4.23	3.63	3.60	3.79			
	1e - 4	<b>3.99</b>	†3.43	2.63	2.32	2.43			
FDE (Solver-3)	1e - 3	8.09	6.29	†5.35	†4.28	†4.27			
	1e - 4	7.66	5.20	†4.25	†2.88	†2.83			
RDE (SciRE-Solver-3)	1e - 3	4.79	3.37	†3.08	†3.18	†3.54			
	1e - 4	4.50	<b>2.70</b>	† <b>2.30</b>	† <b>2.02</b>	<b>2.20</b>			

Table 8: SciRE-Solver-agile with NSR trajectory and starting time 1e - 4.

k	$\phi_1(m) \setminus \text{NFE}$	12	15	20	50	100
CIFAR-10 (VP deep continuous-time model [3])						
k = 3.1	$\phi_1(m) = \phi_1(3)$ $\phi_1(m) = \frac{e-1}{e}$			<b>2.42</b> 2.48		2.48 2.41
k = 2.2	$\phi_1(m) = \phi_1(3)$ $\phi_1(m) = \frac{e-1}{e}$	4.06 6.15	3.34 3.39	2.54 2.57	<b>2.51</b> 2.61	2.42 <b>2.40</b>

our experiments only consider these two extreme cases, i.e., we only choose to allocate m as 3 or directly set  $\phi_1(m) = \frac{e-1}{e}$ . We provide ablation experiments for these two cases in Table 8. In case of  $\phi_1(m) = \frac{e-1}{e}$ , we reach 2.40 FID SOTA value with 100 NFE on CIFAR-10 dataset.

#### E.5 Samples generated on different datasets and some comparisons

In this section, we provide sample comparisons of random sampling using SciRE-Solver, DPM-Solver, and DDIM with the same codebase on different datasets, as depicted in Figs. 6 to 15. Additionally, we present some generated samples on CIFAR-10, CelebA  $64\times64$ , Imagenet  $256\times256$  and Imagenet  $512\times512$ , which reported in Figs. 16 to 23.

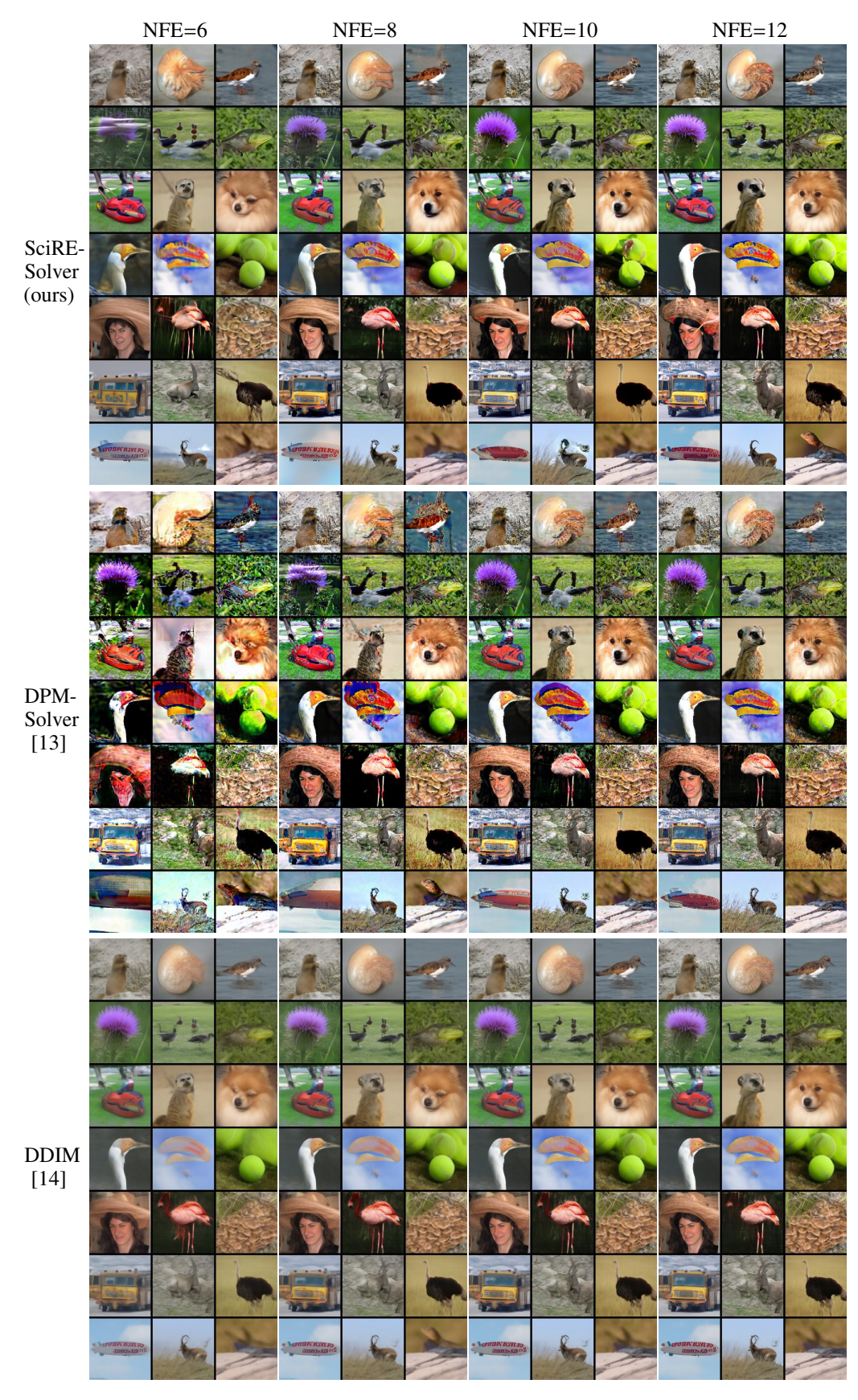


Figure 6: Random samples with the same random seed were generated by SciRE-Solver-2, DPM-Solver-2 [13], and DDIM [14] with the consistently uniform time steps and same settings, employing the pre-trained discrete-time DPM [4] on ImageNet 128×128 with classifier guidance (scale: 1.25).

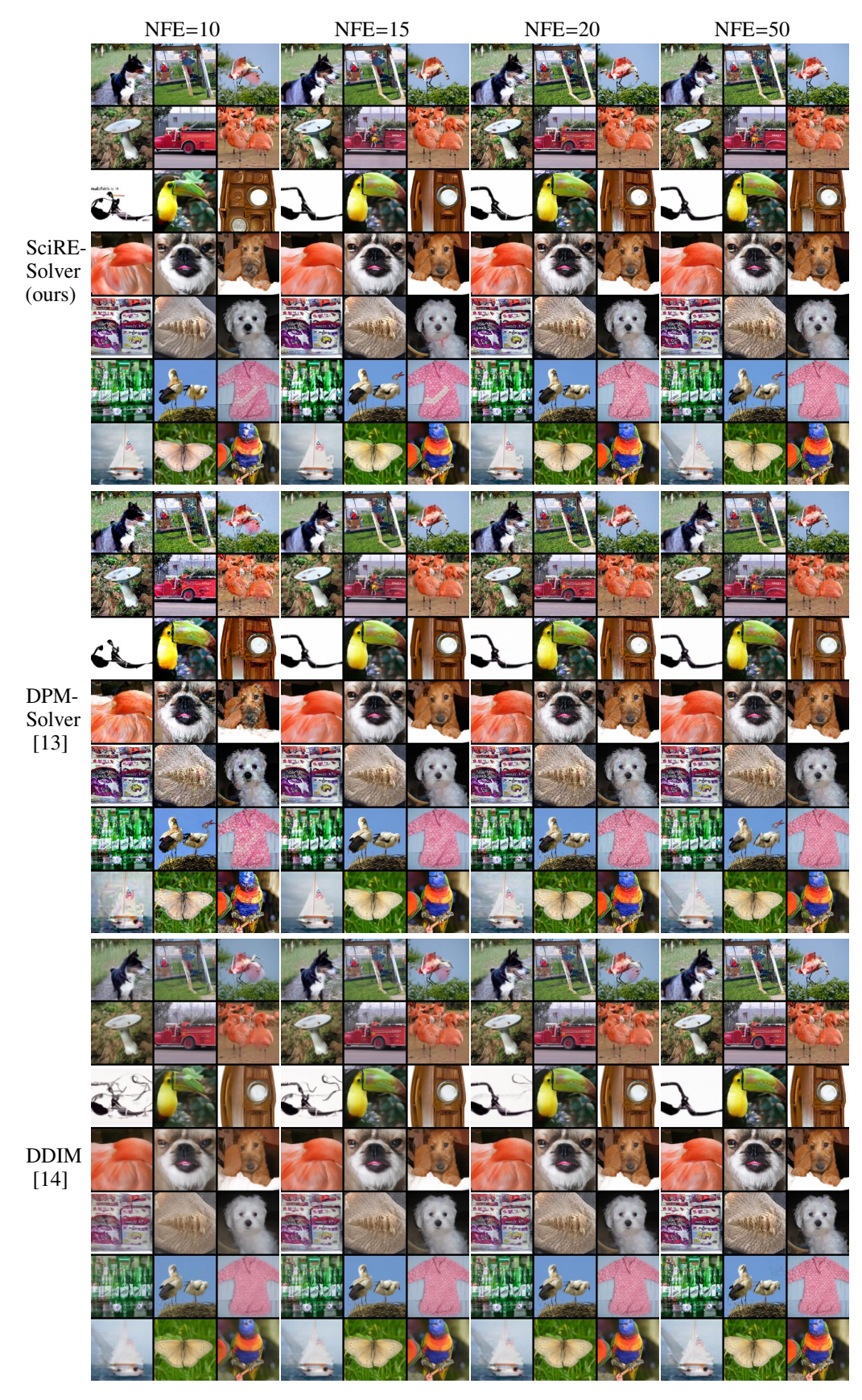


Figure 7: Random samples with the same random seed were generated by SciRE-Solver-2, DPM-Solver-2 [13], and DDIM [14] with the consistently uniform time steps and same settings, employing the pre-trained discrete-time DPM [4] on ImageNet 128×128 with classifier guidance (scale: 1.25).

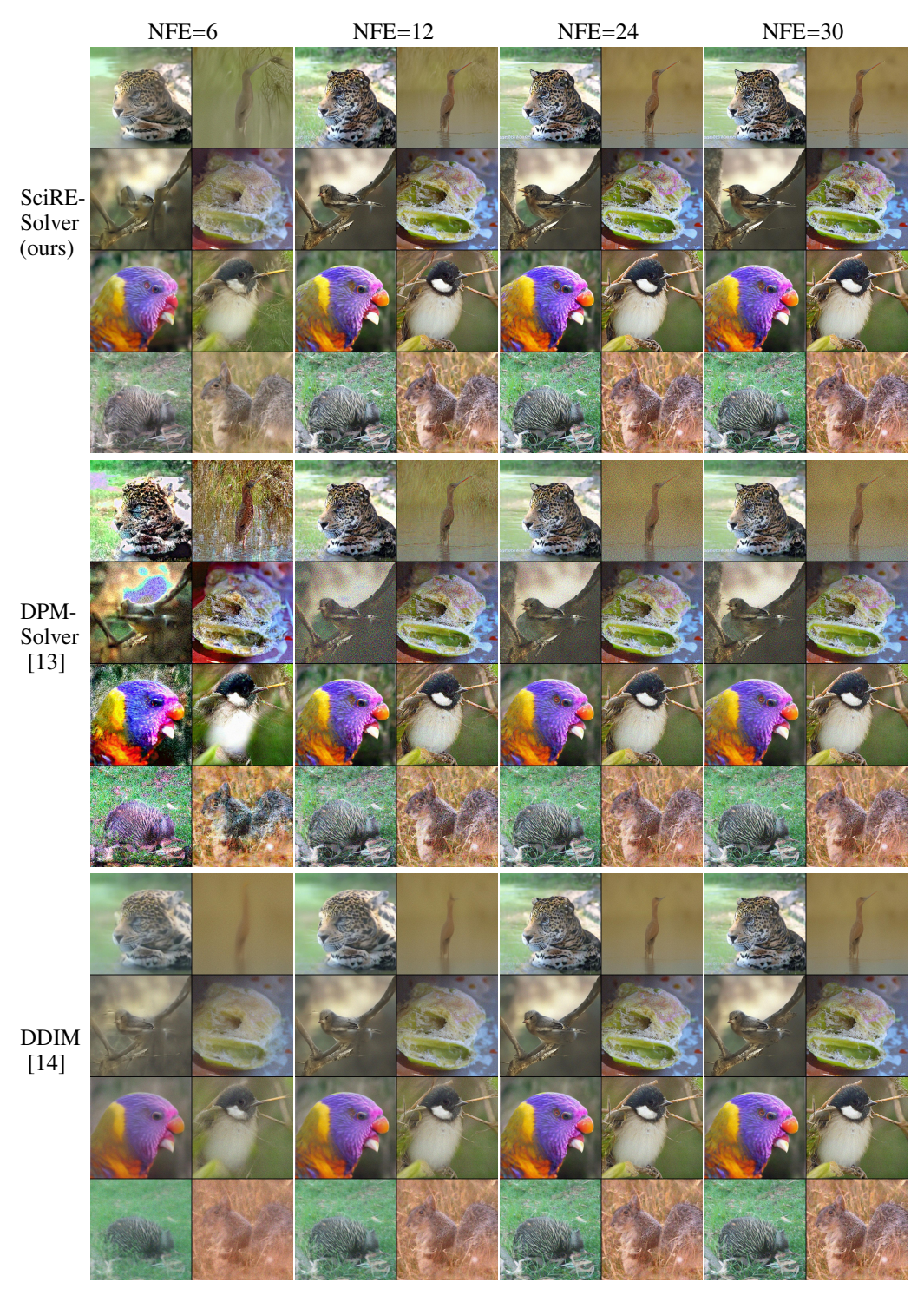


Figure 8: Random samples with the same random seed were generated by SciRE-Solver-2, DPM-Solver-2 [13], and DDIM [14] with the consistently uniform time steps and same settings, employing the pre-trained discrete-time DPM [4] on ImageNet 512×512 with classifier guidance (scale: 1).

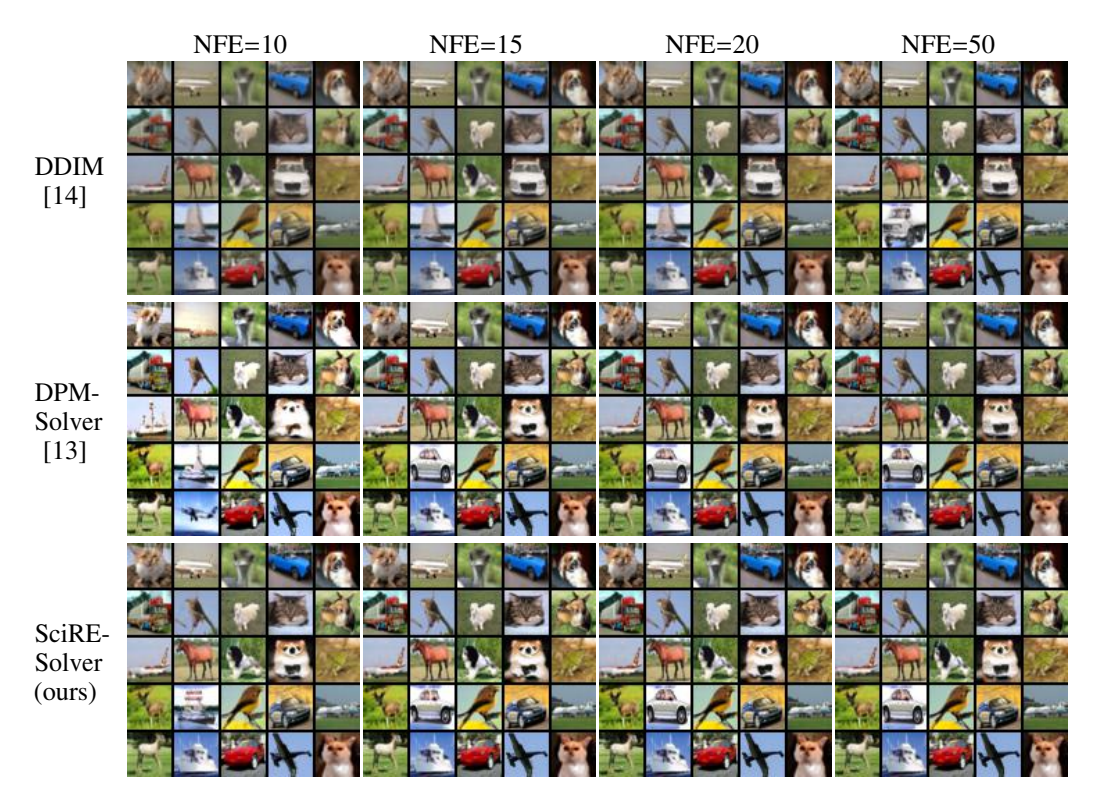


Figure 9: Random samples with the same random seed were generated by DDIM [14] (uniform time steps), DPM-Solver [13] (logSNR time steps), and SciRE-Solver (SNR time steps, k = 3.1), employing the pre-trained discrete-time DPM [2] on CIFAR-10.

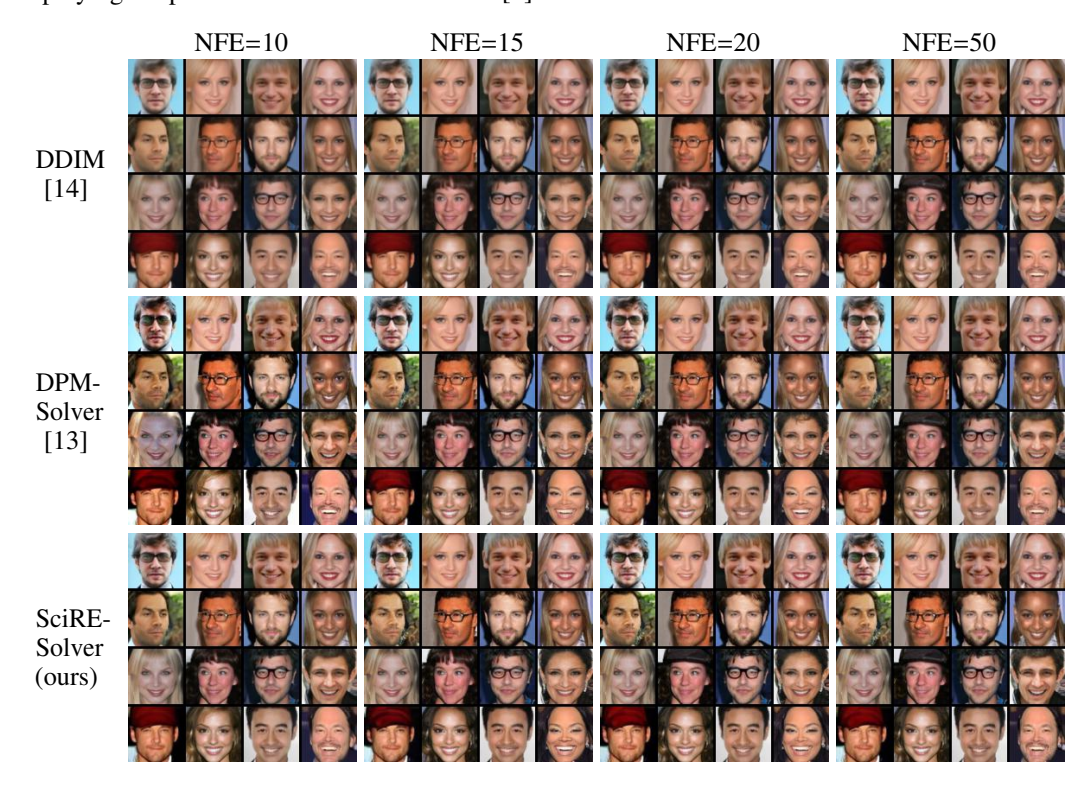


Figure 10: Random samples with the same random seed were generated by DDIM [14] (uniform time steps), DPM-Solver [13] (logSNR time steps), and SciRE-Solver (SNR time steps, k = 3.1), employing the pre-trained discrete-time DPM [14] on CelebA  $64 \times 64$ .

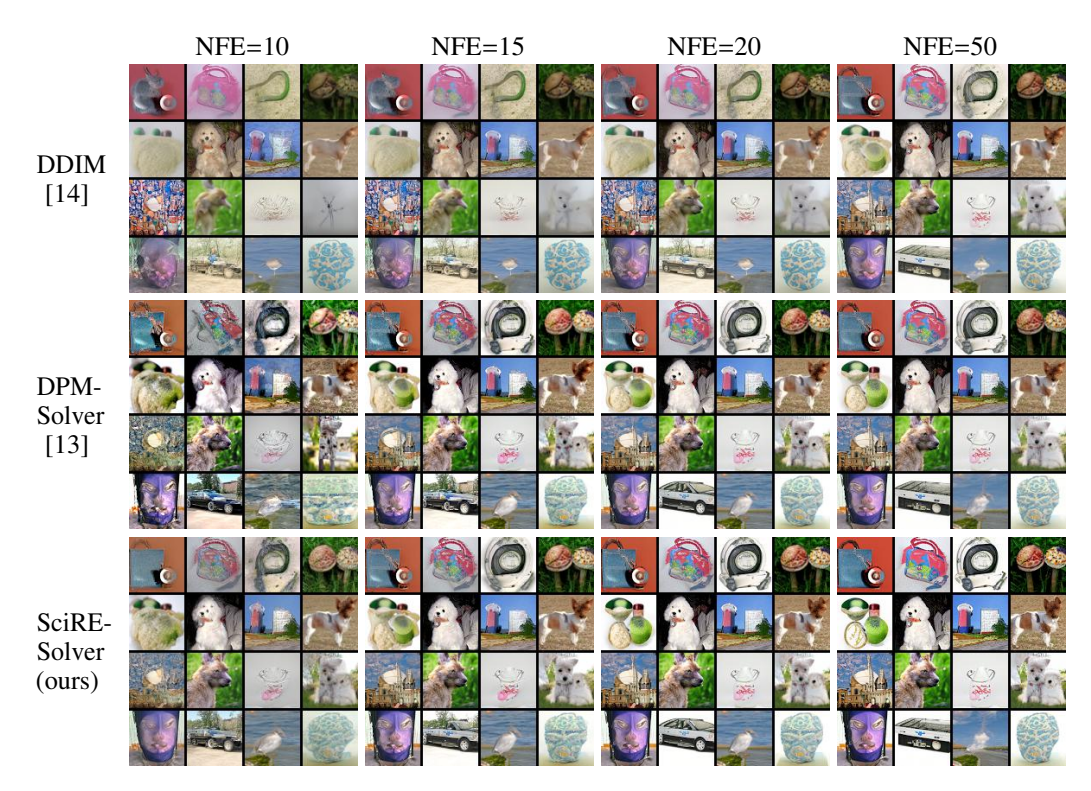


Figure 11: Random samples with the same random seed were generated by DDIM [14] (uniform time steps), DPM-Solver [13] (logSNR time steps), and SciRE-Solver (SNR time steps, k = 3.1), employing the pre-trained discrete-time DPM [19] on ImageNet 64×64.

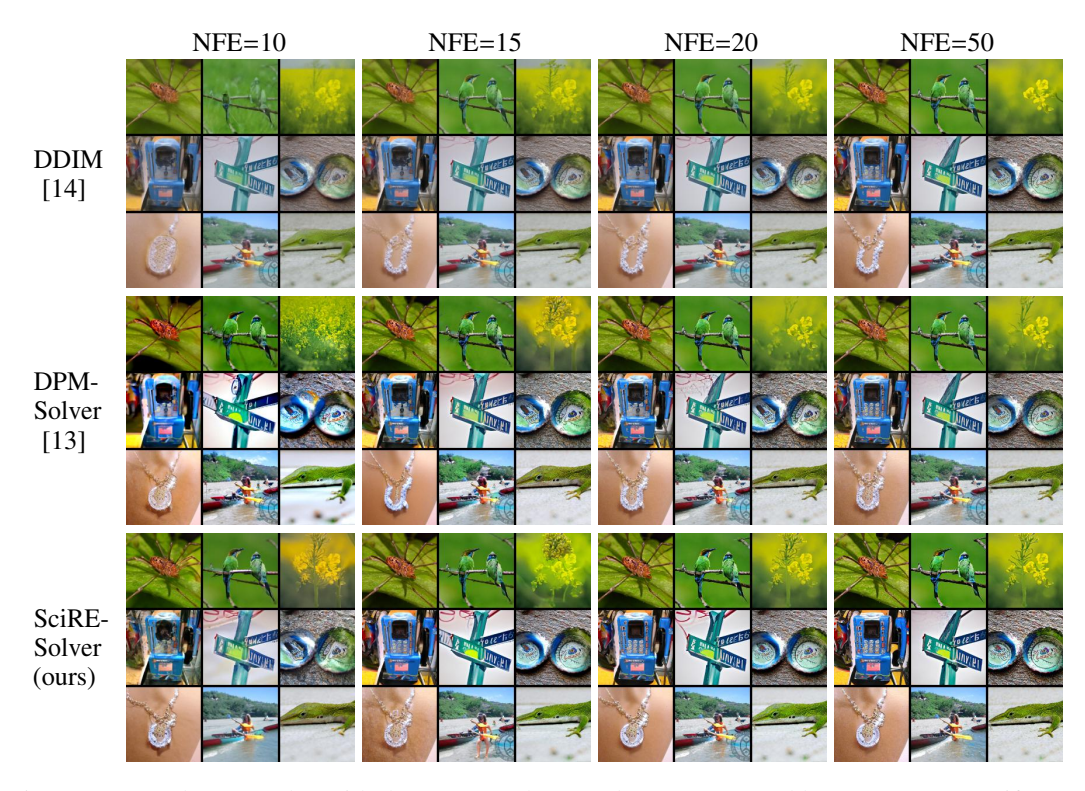


Figure 12: Random samples with the same random seed were generated by DDIM [14] (uniform time steps), DPM-Solver [13] (logSNR time steps), and SciRE-Solver (SNR time steps, k=3.1), employing the pre-trained discrete-time DPM [4] on ImageNet 128×128 (classifier scale: 1.25).

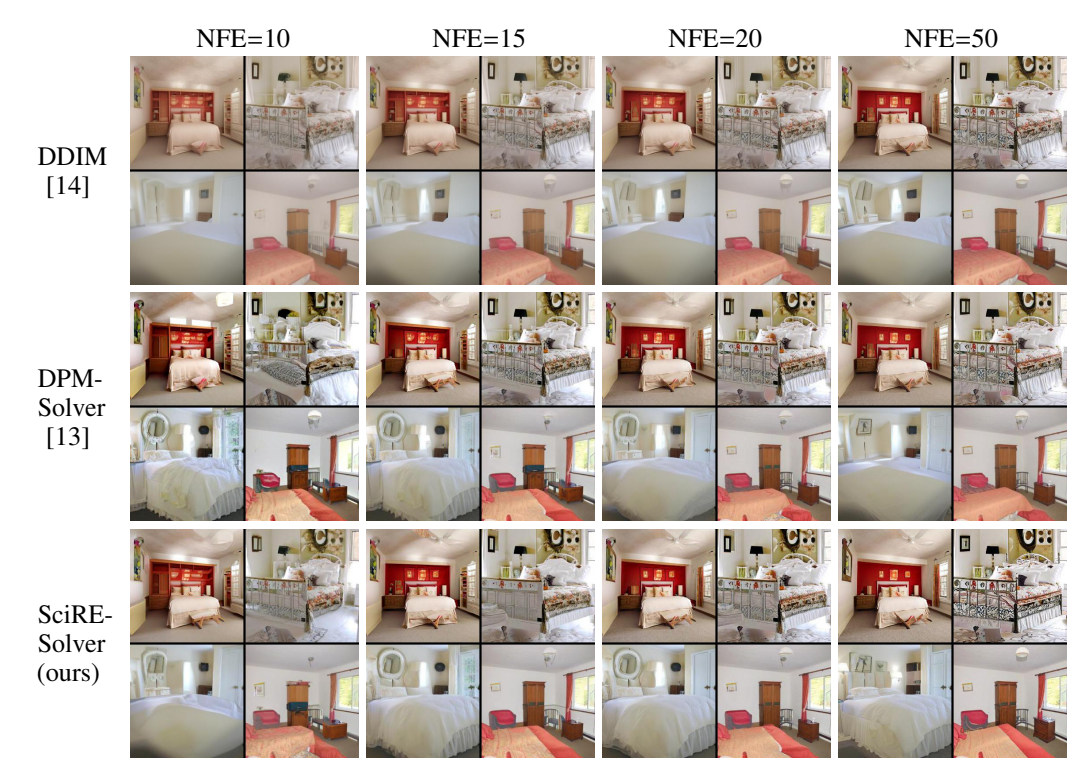


Figure 13: Random samples with the same random seed were generated by DDIM [14] (uniform time steps), DPM-Solver [13] (logSNR time steps), and SciRE-Solver (SNR time steps, k = 3.1), employing the pre-trained discrete-time DPM [4] on LSUN bedroom  $256 \times 256$ .

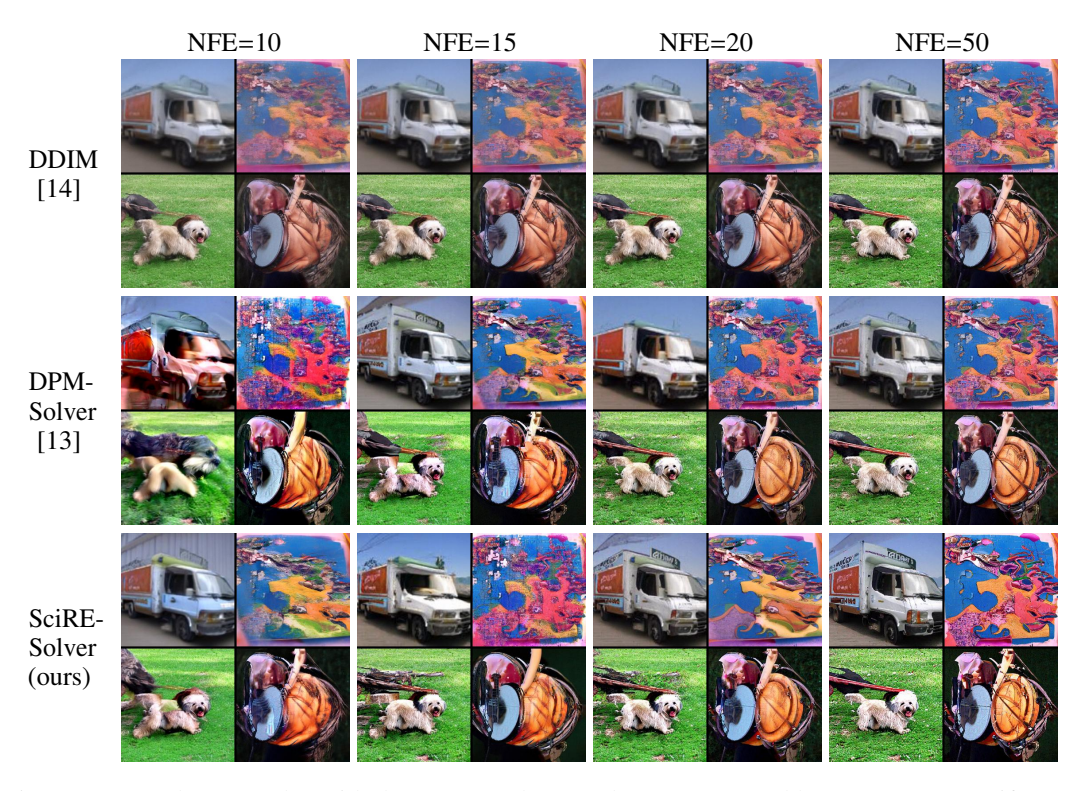


Figure 14: Random samples with the same random seed were generated by DDIM [14] (uniform time steps), DPM-Solver [13] (logSNR time steps), and SciRE-Solver (SNR time steps, k = 3.1), employing the pre-trained DPM [4] on ImageNet 256×256 (classifier scale: 2.5).



Figure 15: Random samples with the same random seed were generated by SciRE-Solver, DPM-Solver [13], and DDIM [14] with the consistently uniform time steps, employing the pre-trained discrete-time DPM [4] on LSUN bedroom 256×256.



Figure 16: Random samples were generated by SciRE-Solver with 12 NFE, employing the pretrained discrete-time DPM [3] on continious-time CIFAR-10. We achieve an 3.48 FID by using the *Sigmoid*-type time trajectory with k = 0.65, and setting the initial time as  $\epsilon = 10^{-3}$ .



Figure 17: Random samples were generated by SciRE-Solver with 20 NFE, employing the pre-trained discrete-time DPM [3] on continious-time CIFAR-10. We achieve an 2.42 FID by using the *NSR*-type time trajectory with k = 3.10, and setting the initial time as  $\epsilon = 10^{-4}$ .



Figure 18: Random samples were generated by SciRE-Solver with 100 NFE, employing the pretrained discrete-time DPM [3] on continious-time CIFAR-10. We achieve an 2.40 FID by using the *NSR*-type time trajectory with k = 3.10, and setting the initial time as  $\epsilon = 10^{-4}$ .



Figure 19: Random samples were generated by SciRE-Solver with 18 NFE, employing the pre-trained discrete-time DPM [14] on CelebA 64×64. We achieve an 2.17 FID by using the *NSR*-type time trajectory with k = 3.10, and setting the initial time as  $\epsilon = 10^{-4}$ .



Figure 20: Random samples were generated by SciRE-Solver-2 with 20 NFE and the uniform time steps, using the pre-trained discrete-time DPM [4] on Imagenet  $512 \times 512$  (classifier scale: 4).



Figure 21: Random samples were generated by SciRE-Solver-3 with 18 NFE and the uniform time steps, using the pre-trained discrete-time DPM [4] on Imagenet  $512 \times 512$  (classifier scale: 1).



Figure 22: Random samples were generated by SciRE-Solver-2 with 20 NFE and the uniform time steps, using the pre-trained discrete-time DPM [4] on Imagenet  $256 \times 256$  (classifier scale: 1).



Figure 23: Random samples were generated by SciRE-Solver-3 with 18 NFE and the uniform time steps, using the pre-trained discrete-time DPM [4] on Imagenet  $256 \times 256$  (classifier scale: 1).